Accepted Manuscript

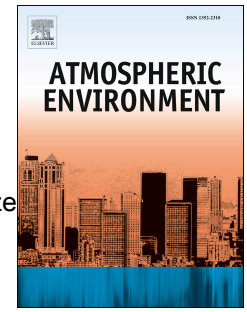

$PM_{2.5}$ and PM_{10} oxidative potential at a Central Mediterranean Site: Contrasts between dithiothreitol- and ascorbic acid-measured values in relation with particle size and chemical composition

Maria Rita Perrone, Ilaria Bertoli, Salvatore Romano, Mara Russo, Gennaro Rispoli, Maria Chiara Pietrogrande

PII: S1352-2310(19)30268-7

DOI: https://doi.org/10.1016/j.atmosenv.2019.04.047

Reference: AEA 16675

To appear in: *Atmospheric Environment*

Received Date: 11 December 2018

Revised Date: 25 March 2019

Accepted Date: 21 April 2019

Please cite this article as: Perrone, M.R., Bertoli, I., Romano, S., Russo, M., Rispoli, G., Pietrogrande, M.C., $PM_{2.5}$ and PM_{10} oxidative potential at a Central Mediterranean Site: Contrasts between dithiothreitol- and ascorbic acid-measured values in relation with particle size and chemical composition, *Atmospheric Environment* (2019), doi: https://doi.org/10.1016/j.atmosenv.2019.04.047.

$PM_{2.5}$

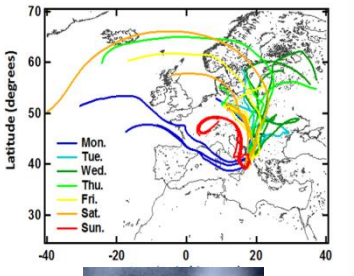

PM_{10}

Dithiothreitol Assay

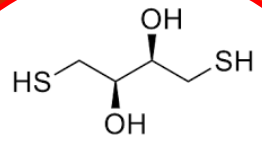

Oxidative Potential

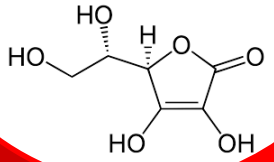

Ascorbic Acid Assay

$PM_{2.5}$ and PM_{10} Oxidative Potential at a Central Mediterranean Site: Contrasts between Dithiothreitol- and Ascorbic Acid-Measured Values in Relation with Particle Size and Chemical Composition

Maria Rita Perrone[1], Ilaria Bertoli[2], Salvatore Romano[1], Mara Russo[2], Gennaro Rispoli[1], Maria Chiara Pietrogrande[2*]

[1]Department of Mathematics and Physics, University of Salento,
Via per Arnesano, 73100 Lecce, Italy

[2]Department of Chemical and Pharmaceutical Sciences, University of Ferrara,
Via Fossato di Mortara 17/19 - 44121 Ferrara, Italy

*Corresponding author: Prof. M.C. Pietrogrande, email: mpc@unife

Highlights

- Oxidative potential was assessed for $PM_{2.5}$ at a Central Mediterranean Site.
- Oxidative potential and chemical composition of $PM_{2.5}$ and PM_{10} were compared.
- The dependence of the OP^{DTT} and OP^{AA} responses on seasons were investigated.
- OP^{DTT} were similar in $PM_{2.5}$ and PM_{10} and highly associated with OC, EC and K^+.
- OP^{AA} were higher in PM_{10} than in $PM_{2.5}$ and highly associated with Cu and Fe.

Keywords

Oxidative potential; $PM_{2.5}$ particulate matter; $PM_{2.5}$ and PM_{10} size distribution, Dithiothreitol assay; Ascorbic acid assay; $PM_{2.5}$ and PM_{10} chemical composition.

Abstract

In this study, $PM_{2.5}$ airborne particulate matter was collected over a full year at a costal site of the Central Mediterranean Sea and analyzed for its chemical composition and oxidative potential (OP), determined by the dithiothreitol (DTT) and the ascorbic acid (AA) assays. In autumn-winter, the volume normalized oxidative OP (OP_V) were 0.29±0.03 nmol min^{-1} m^{-3} and 0.21±0.03 nmol min^{-1} m^{-3} for the DTT (OP^{DTT}_V) and AA (OP^{AA}_V) assay, respectively. In spring-summer the OP^{DTT}_V values were higher than OP^{AA}_V responses, i.e., 0.19±0.02 nmol min^{-1} m^{-3} vs. 0.09±0.01 nmol min^{-1} m^{-3}. Overall, marked seasonality was observed with higher values in Autumn-Winter (AW) than in Spring-Summer (SS), i.e., 1.5 and 2.3 times increase for OP^{DTT}_V and OP^{AA}_V, respectively.

In the cold season, the OP_V activity was broadly correlated with metals and carbon species, such as K^+, NO_3^-, Ba, Cd, Cu, Fe, Mn, P, V, OC, EC, Acetate, Oxalate and Glycolate ($p<0.05$). This suggested the main contribution of a "mixed anthropogenic" source, consisting of the biomass burning (K^+, OC and EC) and traffic (Ba, Cu, Fe, Mn, V, EC) emissions. In SS, OP_V was significantly correlated with only few species i.e., OC, EC, Cu, and NO_3^-, suggesting main association with the "mixed anthropogenic" and the "reacted dust" sources.

For each sampling day, $PM_{2.5}$ and PM_{10} samples were simultaneously collected and analyzed to investigate the variation of the OP activity in relation with the particle size and chemical composition.

OP^{DTT}_V values exhibited a poor particle-size dependence, with similar values close to 0.20±0.04 nmol min^{-1} m^{-3} in both fractions. This could be explained by the association of OP^{DTT}_V with species mainly accumulated in the fine fraction, i.e., OC, POC and EC and K^+. Otherwise, the OP^{AA}_V responses exhibited a clear particle-size dependence, with significantly higher values for PM_{10} than for $PM_{2.5}$, i.e., 0.35±0.06 vs. 0.21±0.03 nmol min^{-1} m^{-3} in AW and 0.23±0.04 vs. 0.09±0.01 in SS. This may be supported by the strong correlation of OP^{AA}_V with Cu and Fe, which were most abundant metals in the PM_{10} fraction.

The data of specific monitoring days were investigated in detail to better highlight the impact of some individual redox active species on the OP^{DTT}_V and OP^{AA}_V responses.

Capsule

The oxidative potential of $PM_{2.5}$ and PM_{10} samples was assessed with Dithiothreitol and Ascorbic Acid assays: the variation of OP responses was related with the PM size and chemical composition.

Introduction

The interest on the health effects associated with the air particulate matter (PM) has been growing over the last few decades. In fact, the exposure to PM has been linked to adverse health effects, such as respiratory and cardiovascular diseases, through the production of reactive oxygen species (ROS) in the human respiratory tract (Bates et al., 2015; Kelly, 2003; Mittal et al., 2014; Samara, 2017 and references therein; Venkatachari and Hopke, 2008). These ROS could be carried either by the PM themselves or generated via interactions between particle-bound redox-active components and lung lining fluid (Poschl and Shiraiwa, 2015). Therefore, the oxidative potential (OP), defined as the capacity of PM to cause damaging oxidative reactions, has been suggested as an additional PM indicator, that would encompass the PM toxicological response (Pietrogrande et al., 2018a and references therein). The compounds likely implicated in the ROS formation include organic carbon, polycyclic aromatic hydrocarbons, quinones (Cho et al., 2005; Janssen et al., 2015; Lyu, et al., 2018; Verma, et al., 2015), and also soluble species, particularly transition metals such as iron, copper, and vanadium (Charrier and Anastasio, 2012; Crobeddu, et al., 2017; Fang et al., 2017; Shuster-Meiseles et al., 2016; Valko et al., 2005). Among the most used acellular methods for assessing PM OP, the dithiothreitol (OP^{DTT}, Charrier and Anastasio, 2012) and the ascorbic acid (OP^{AA}, Mudway et al., 2004) depletion assays display the advantage of using low-cost spectrophotometric UV-Vis measurements (Calas et al., 2018; Crobeddu et al., 2017). These assays have been found to display different sensitivity towards the redox-active species present in PM (Calas et al., 2018; Fang et al., 2016; Janssen et al., 2015; Visentin et al., 2016; Weber et al., 2018; Yang et al., 2014). Using these assays, some authors of this study assessed the OP^{DTT} and OP^{AA} activity of $PM_{2.5}$ and PM_{10} samples collected at different sites across Italy (Visentin et al. 2016; Pietrogrande et al., 2018a; Pietrogrande et al., 2018b).

Additionally, particle-size has been found critical in mediating PM toxicity, with particular attention to $PM_{2.5}$ and PM_{10} particles, for which the European Union has defined target values of mass concentrations in the Air Quality Directives in order to improve air quality (CEC, 2008). $PM_{2.5}$ has been found more potent than larger PM_{10}, because of its increased number, large surface area and high pulmonary deposition efficiency (Chalupa et al., 2004). The dependence of the OP responses on the PM size has been investigated, mainly for PM_{10} and $PM_{2.5}$ (Boogaard et al., 2012; Chirizzi et al., 2017; Daher, et al., 2014; Fang et al., 2017; Jaafar et al., 2014; Janssen et al. 2014; Lyu, et al., 2018; Shafer et al., 2016; Simonetti et al., 2018).

This paper assesses OP of $PM_{2.5}$ and PM_{10} samples simultaneously collected at a peninsular site of the Central Mediterranean basin, which is impacted by different sources, because of the

contributions of long-range-transported air masses from the surrounding regions (Perrone et al., 2013; 2014a, 2014b, 2016; Becagli et al., 2017; Chirizzi et al., 2017).

In this study, the responses from the DTT and AA assays are investigated and compared in order to associate the variation in the OP activity with the particle size and distribution of the redox-active species in $PM_{2.5}$ and PM_{10} fractions. Therefore, the findings of this work would provide relevant insight in identifying the PM sources that mostly influence the oxidative properties of the PM size fractions.

1. Materials and Methods

2.1. Sampling Site and Period

The study site is located in a suburban site (40.3°N; 18.1°E) of the flat Salento's peninsula, in the Central Mediterranean. Thirty-nine $PM_{2.5}$ filters collected from 5th December 2014 until 12th October 2015 have been analysed: more specifically, 24 samples from April to September (Spring-Summer, SS) and 15 in October–March months (Autumn-Winter, AW). Sampling was performed with a low volume (2.3 m^3 h^{-1}) HYDRA-FAI dual-sampler that made it possible to simultaneously collect $PM_{2.5}$ and PM_{10} granulometric fractions using two independent sampling lines. Note that the PM_{10} samples of this study were included in a more extended study devoted to 53 PM_{10} filters, as previously reported in Pietrogrande et al. (2018a).

The sampler was located at the Mathematics and Physics Department of the University of Salento (~10 m above ground level) to collect 24-hour $PM_{2.5}$ samples on 47-mm-diameter preheated filters (PALLFLEX, Tissuquartz). The filters were conditioned for 48 hours (25°C and 50% humidity) before and after sampling and the PM mass concentrations were determined by the gravimetric method. Uncertainties on mass concentrations are lower than 5%. The $PM_{2.5}$ loaded filters were divided in four punches for the determination of inorganic ions and methanesulfonate, metals, organic and elemental carbon, and the oxidative potential.

2.2. Ions, Metals, and Organic and Elemental Carbon Analyses in the PM Samples

Loaded as well as blank $PM_{2.5}$ filters were submitted to different analyses to characterize their chemical composition by using the methods described in detail in Perrone et al. (2014a) and Pietrogrande et al. (2018a). In particular, anions (Cl^-, NO_2^-, NO_3^-, SO_4^{2-}, MSA^-, oxalate, acetate, glycolate, proponiate, formate, and pyruvate) and cations (Na^+, NH_4^+, K^+, Mg^{2+}, Ca^{2+}) mass

concentrations were determined by a Flow Analysis Ion Chromatography (FA-IC). An Inductively Coupled Plasma Atomic Emission Spectrometer was used to determine the mass concentration of Al, Ba, Cd, Ce, Co, Cr, Cu, Fe, La, Mn, Mo, Ni, P, Pb, Sr, Ti, V, and Zn. Ion and metal analyses were performed at the Chemistry Department of the University of Florence. The Sunset Carbon Analyzer Instrument with the EUSAAR-2 temperature program protocol (Cavalli et al., 2010) was used to determine the organic and elemental carbon (OC and EC, respectively) mass concentrations.

2.3. Assessment of the PM Oxidative Potential

The OP of the collected $PM_{2.5}$ samples was assessed with the DTT and AA acellular methods. The OP response was measured as the antioxidant depletion rate of known quantity of DTT and AA, following the experimental procedure described in Pietrogrande et al. (2018a, b).

The DTT and AA depletion rates (nmol min^{-1}) were determined by linear fitting of the reagent concentration versus time relationship (five experimental points at 5, 10, 15, 25, 40 minutes) plot. In general, a good linearity was found with correlation coefficient $R^2 \geq 0.98$ (Visentin et al., 2016). For both methods, the DTT or AA depletion rates were determined for blank quartz filters and subtracted from response of each real PM sample. Sample and blank assays were run in duplicate.

3. Results

3.1. $PM_{2.5}$ mass concentration and chemical composition

The chemical composition of $PM_{2.5}$ particles was characterized in detail for more than 30 species, including ions − Na^+, NH_4^+, K^+, Mg^{2+}, Ca^{2+}, Cl^-, NO_2^-, NO_3^- and SO_4^{2-} − metals – Al, Ba, Cd, Ce, Co, Cr, Cu, Fe, La, Mn, Mo, Ni, Pb, Sr, Ti, V and Zn – and organic components, – OC and EC, methanesulfonate ion and carboxylic ions. The measured $PM_{2.5}$ mass concentrations are reported in Table S1 of the Supplementary Information (SI), as the mean values and corresponding standard errors of the mean (SEM) computed for AW and SS period, separately. Such a grouping is motivated by the season dependence of the PM mass concentration and chemical composition at the study site, as reported in previous studies (e.g., Perrone et al., 2014a, 2016; Pietrogrande et al., 2018a). The two-tail t-test was applied to the mean AW and SS values to assess their statistical difference at $p < 0.05$ significance level (values marked by * in Table S1).

The mean $PM_{2.5}$ mass concentration varied weakly with seasons being 26±2 and 20±1 μg m^{-3} in AW and SS, respectively. This result may be related to the weak dependence on seasons of the

166 planetary boundary layer (PBL) depth in the study area, as reported in previous studies (Perrone et
167 al., 2013, 2014b, 2016, Perrone and Romano, 2018). The percentage contribution of the investigated
168 species to the total $PM_{2.5}$ and PM_{10} mass are summarized in Figure 1 for AW and SS data (Fig. 1a-c
169 and 1b-d, respectively). OC was discriminated between primary (POC) and secondary organic
170 carbon (SOC) by using the OC/EC ratio approach (Pio et al., 2011). The mass percentages due to
171 metals and to MS^- and carboxylic ions have been grouped in Met and Cxi, respectively. Among the
172 analysed species, the carbonaceous compounds are the major components. SO_4^{2-}, NO_3^-, NH_4^+ and
173 K^+ are by far the most abundant inorganic ions, while metals are minor components.
174 The higher levels of EC, POC, NO_3^-, and K^+ in AW than in SS can be related to the stronger
175 contribution from residential heating in the cold season. The greater mass concentration of Na^+,
176 NH_4^+, Mg^{2+}, Ca^{2+}, SO_4^{2-}, and SOC in SS than in AW may be related to the meteorological
177 conditions occurring in SS over the Mediterranean, mainly the formation of secondary particles
178 favoured by the large solar irradiance and the dust resuspension because of the lack of rainy days
179 (e.g. Perrone et al., 2013, 2014a).
180
181 *3.2. $PM_{2.5}$ and PM_{10} samples: comparisons between mass concentrations and chemical*
182 *components*
183
184 The $PM_{2.5}$ chemical composition was compared with that of the simultaneously collected PM_{10}
185 samples, which are a subset of the overall data reported in Pietrogrande et al (2018a). The mean
186 PM_{10} mass concentration was 34±3 and 28±2 μg m^{-3} in AW and SS (Table S1), confirming the
187 prevalent contribution of fine particles at the study site, i.e., $PM_{2.5}$ accounted for 77 and 70% of the
188 PM_{10} mass, in AW and SS, respectively (Perrone et al., 2013, 2014a). Accordingly, the distribution
189 of all the investigated chemical species showed the same seasonal trend in PM_{10} as in $PM_{2.5}$
190 fractions (e.g., Perrone et al., 2013, 2014a, 2014b; Pietrogrande et al. 2018a), as clearly depicted in
191 Figure 2 (compare Fig. 2a and 2b with Fig. 2c and 2d, respectively). In particular, carbonaceous
192 compounds showed similar concentration in both fractions being accumulated in the fine PM
193 (Jaafar et al. 2014; Lovett et al. 2018). Accordingly, the OC/EC ratios computed in both PM
194 fractions were similar in SS and AW, respectively (Table S1) (Waked et al., 2014). In addition,
195 SO_4^{2-} and organic secondary ions have similar concentrations in both fractions, as they preferentially
196 concentrate in the accumulation mode due to their secondary nature (Daher et al., 2014).
197 Conversely, the NO_3^- ion showed an unexpected size distribution with higher concentration in PM_{10}
198 than in $PM_{2.5}$, as previously found in most coastal sites of the southern Mediterranean Basin (e.g.,
199 Bardouki et al., 2003; Perez et al., 2008). It is probably due to the low thermal stability of NH_4NO_3

in SS, when the formation of HNO_3 instead of NH_4NO_3 is favoured under the prevalent warm conditions of most of the Central Mediterranean sites (Querol et al., 2008). The presence of gaseous HNO_3 and the possible interaction of the pollutant with mineral calcium carbonate, K^+, and sea salt may account for the increase of the coarse nitrate proportion (Perrone et al., 2013; Perrone et al., 2019). Fine nitrate particles are usually the result of nitric acid/ammonia reactions leading to the formation of ammonium nitrate. The concentrations of Cl^- and Na^+ (tracers of sea salt aerosol) and Mg^{2+} and Ca^{2+} (crustal tracers of soil resuspension) were nearly twice in PM_{10} compared with $PM_{2.5}$, that is consistent with the nature and size of these particles (Hasheminassab et al., 2014). As expected, also metal species, are accumulated in the coarse fraction, i.e., Al, Ba, Ce, Cu, Fe, with Fe, Zn and Cu as the dominant metal species (Lyu et al., 2018; Pant et al., 2015; Shirmohammadi et al., 2017; Simonetti et al., 2018; Waked et al., 2014).

3.2.1. Source apportionment of $PM_{2.5}$ and PM_{10} particles

Although the small number of the present $PM_{2.5}$ samples prevents a source apportionment study, to describe the source contribution to PM mass we can use the factors computed from Positive Matrix Factorization (PMF) in a recent study concerning overall 90 $PM_{2.5}$ and PM_{10} samples collected at the study site (Perrone et al., 2019) of which the present 39 samples represent a randomly selected subset. It well represents the whole dataset, as for each investigated species, the computed mean concentrations show a good agreement (within ± 1 SEM) (Table S1) with those of the all dataset (Perrone et al., 2019). For convenience, the PMF results are summarized in Table 1, reporting the 6 identified factors/sources with the corresponding percentage contributions in AW and SS, respectively. The "sulphate" source was associated to the high percentage of SO_4^{2-}, NH_4^+, and Pb. The "mixed anthropogenic" source was related to markers from both traffic (e.g., EC, OC, Cu, Fe, Ba) and biomass burning (e.g., K^+, OC, EC). The "heavy oil/secondary marine" source was dominated by V, Ni, and Cr, likely due to ship emissions, and MS^-. The "reacted dust" factor was related to crustal particles mixed with nitrate and sulphate secondary specie. The "sea salt" source was characterized by the main markers Na^+ and Cl^-. The "soil dust" source was mainly associated with soil related species, i.e., Al, Ca^{2+}, Sr, Ti, Fe, Mn.

3.3. Oxidative potential of $PM_{2.5}$ samples

The $PM_{2.5}$ OP responses were measured with both assays (OP^{DTT}: nmol min^{-1} and OP^{AA}: nmol min^{-1}) and normalized by the volume of sampled air ($OP^{DTT}{}_V$ and $OP^{AA}{}_V$ expressed as nmol min^{-1} m^{-3}) as

an exposure metrics accounting for inhaled air. In addition, OP^{DTT} and OP^{AA} were normalized by the $PM_{2.5}$ mass (OP^{DTT}_m and OP^{AA}_m expressed as nmol min^{-1} μg^{-1}) to point out the intrinsic ability of the particles to deplete physically relevant antioxidants. Figure 2 reports the time series of the OP^{AA}_V and OP^{DTT}_V activity measured in the different particle size fractions ($PM_{2.5}$: dark grey bars; PM_{10}: light grey bars) during the cold (AW, Figures 1a, c) and the warm period (Figures 1b, d).

Overall, the OP^{DTT}_V responses were higher than the OP^{AA}_V ones in both seasons. More specifically, in AW, the mean OP^{DTT}_V value was 0.29±0.03 nmol min^{-1} m^{-3} and the mean OP^{AA}_V value was 0.21±0.03 nmol min^{-1} m^{-3}. In SS, the difference was larger, with OP^{DTT}_V responses of 0.19±0.02 nmol min^{-1} m^{-3} and OP^{AA}_V of 0.09±0.01 nmol min^{-1} m^{-3}.

The measured OP^{DTT}_V values are in reasonable agreement with the mean value (0.40±0.26 nmol min^{-1} m^{-3}) reported by Chirizzi et al. (2017) for the same site by analyzing 30 $PM_{2.5}$ samples collected in AW between 2013 and 2016. In general, our results are towards the lowest end of the range of values reported in literature for $PM_{2.5}$ particles, being the study site away from large sources of local pollution. This may represent a peculiarity of the results reported in the paper, as most of the literature data concern OP at large urban and/or polluted sites. Consequently, the OP^{DTT}_V varied from 0.3 nmol min^{-1} m^{-3} in Atlanta to 2.0 nmol min^{-1} m^{-3} in Rotterdam (Janssen et al., 2014; Lyu, et al., 2018; Samara, 2017), while the OP^{AA}_V ranged from 0.3 to 20 $nmol^{AA}$ min^{-1} m^{-3} (Fang et al. 2016; Janssen et al., 2014; Weber et al., 2018).

Overall, the two assays displayed similar sensitivity to the studied $PM_{2.5}$ samples (Table 2), as proved by the significant correlation ($p < 0.01$) between OP^{DTT}_V and corresponding OP^{AA}_V responses in both seasons (r= 0.91 and r= 0.70, for AW and SS, Table 3). This is in agreement with some results reported in literature (e.g., Janssen et al. 2014; Mudway et al. 2004). But, it is in contrast to other papers reporting different sensitivity of the two assays towards the same redox-active species (Calas et al., 2018; Fang et al, 2016; Simonetti et al., 2018; Szigeti at al., 2016; Visentin at al., 2016; Weber et al., 2018; Yang et al., 2014). Indeed, the specific sensitivity of OP^{DTT} OP^{AA} responses is still an open question. The results of the present study may likely contribute to elucidate this point.

Despite the similarity of the mean OP^{DTT}_V and OP^{AA}_V responses (Table 2) and the overall good correlation between the data, the individual OP^{DTT}_V and OP^{AA}_V values largely varied day-by-day with different behaviour for the same sample, as shown by the daily trend reported in Figures 2 a-d (dark grey bars). Such a large variability may be likely ascribed to the day-by-day change of the $PM_{2.5}$ concentration/composition, because of the impact at the study site of long-range transported particles from the surrounding regions. Such an impact has been found by the Authors by investigating the main airflows by using the Hybrid Single-Particle Lagrangian Integrated

Trajectory (HYSPLIT) model version 4.8, from NOAA/ARL (Draxler and Hess 1998) (Perrone et al., 2013; 2014a, 2014b, 2016; Becagli et al., 2017; Chirizzi et al., 2017; Pietrogrande et al., 2018a). This represents an additional peculiarity of paper's results, as most of the previous studies were mainly devoted to sites mainly impacted by local-pollution sources, e.g. traffic sites, underground train stations, farms, as mentioned (Boogaard et al., 2012; Calas et al., 2018; Jaafar et al., 2014; Janssen et al., 2014; Moreno et al., 2017; Shafer et al., 2016; Shuster-Meiseles et al., 2016; Simonetti et al., 2018; Weber et al., 2018; Zhang et al., 2017).

The comparison of the OP^{DTT}_V and OP^{AA}_V values (Figures 2a-d, dark grey bars) with the corresponding $PM_{2.5}$ mass concentrations (Fig. 2e,f, dark grey bars) revealed that high OP_V values were associated with high $PM_{2.5}$ mass concentrations, indicating that the OP_V responses were extensive parameters dependent on $PM_{2.5}$ mass concentrations. This is described by the good linear correlation ($p < 0.001$) of both the OP^{DTT}_V and OP^{AA}_V values with the $PM_{2.5}$ mass: the Pearson correlation coefficients are 0.79 and 0.63 ($p < 0.001$) for OP^{DTT}_V in AW and SS respectively, and 0.82 ($p < 0.001$) for OP^{AA}_V in AW. Consistently, the OP^{DTT}_m response was nearly constant through the investigated period, with mean value of 0.010±0.001 nmol min^{-1} μg^{-1} (Table 2). The OP^{AA}_V values were less significantly (r=0.47, $p < 0.002$) correlated with the $PM_{2.5}$ mass in SS. Therefore, the mean OP^{AA}_m responses changed through the year, with significantly higher values in AW (0.008±0.001 nmol min^{-1} μg^{-1}) compared with SS (0.005±0.001 nmol min^{-1} μg^{-1}). Janssen et al., (2014) also found significant correlations between the $PM_{2.5}$ mass concentration and OP^{DTT}_V.

As OP responses were measured over a full year, the OP seasonal trend was investigated and related with the particle chemical composition. Significantly higher OP^{DTT}_V and OP^{AA}_V responses were measured in the cold than in warm seasons, as supported by a two-tail *t*-test on AW and SS mean values (significant differences at $p < 0.05$ level are marked by * in Table 2). More specifically, the average OP^{DTT}_V and OP^{AA}_V values were 1.5 and 2.3 times higher in the cold period than in the warm period, respectively. Such a seasonality of OP^{DTT}_V and OP^{AA}_V values has been also observed in other studies for ambient $PM_{2.5}$ samples and related to seasonal changes of the PM chemical composition (Fang et al., 2016; Verma et al., 2015; Visentin et al., 2016; Weber et al., 2018).

3.4. Association of the oxidative potential with chemical components/sources

To identify the $PM_{2.5}$ chemical components and hence the pollution sources driving ROS activity, the association between the OP^{DTT}_V and OP^{AA}_V responses and the concentrations of chemical species was investigated by correlation analysis. The Pearson correlation coefficient (r) was

computed for each investigated component for AW and SS, separately, and reported in Table 3 (r values significant at $p < 0.05$ level are in bold).

In the cold season both OP responses were widely correlated with several species, namely, K^+ and NO_3^-, several metals (Ba, Cd, Cu, Fe, Mn, P, V), and carbonaceous species (OC, EC, Acetate, Oxalate and Glycolate). In SS samples OP showed significant correlation with only few species, i.e., NO_3^-, Cu, OC and EC.

In addition, the inter-correlation among the analysed species was investigated to highlight association among common emission sources and/or secondary processes (correlation coefficient r reported in Tables S2 and S3 of the Supplementary Information for AW and SS, respectively). One observes that in AW all the species highly correlated with OP^{DTT}_V and/or OP^{AA}_V also showed a significant inter-correlation. In SS, the species NO_3^-, Cu, OC and EC were highly inter-correlated, but their correlation with K^+, Ba, Cd, Fe, Mn, P, V, OC, Acetate, Oxalate and Glycolate was rather weak (Table S3).

By combining these data with the PMF results, we can infer that in both seasons OP was mainly associated with the "mixed anthropogenic" source, including traffic and biomass burning, and also with the "reacted dust" factor (Table 1). Therefore, the smaller OP values observed in SS were likely explained by the lower contribution of the "mixed anthropogenic" source, which decreased from 55.3% to 15.9% from AW to SS (Table 1).

These results are consistent with several literature data on $PM_{2.5,}$ that report the dominant contribution to OP_v of carbon components from biomass combustion (Fang, et al., 2016; Janssen et al., 2014; Muciga et al., 2009; Reid et al., 2005; Styszko et al., 2017; Verma et al., 2015; Zhang et al., 2017), as well as of traffic related metals, such as road dust components, vehicular abrasion metals and fuel oil combustion emissions (Crobeddu et al, 2017; Daher et al., 2014; Lyu,et al, 2018; Moreno et al, 2017; Shafer, et al, 2016; Shirmohammadi et al., 2017; Shuster-Meiseles et al., 2016; Valko et al., 2005; Yang et al., 2014).

3.5. OP^{DTT} and OP^{AA} responses for $PM_{2.5}$ and PM_{10} fractions

The variation of the OP activity in $PM_{2.5}$ and PM_{10} fractions was investigated in relation with the PM chemical composition/source. The presented $PM_{2.5}$ data were compared with the PM_{10} results measured in a previous work for the subset of this study. Concentrations of the investigated constituents (Figure 2e-f and Table S1 of SI) and OP responses (Table 2 reports mean ± SEM values, significant differences at $p < 0.05$ between the $PM_{2.5}$ and PM_{10} are marked in bold) were compared in Pietrogrande et al. (2018a).

The DTT assay produced similar responses for both size fractions, i.e., 0.24±0.04 and 0.29±0.03 nmol min^{-1} m^{-3} in AW, and 0.22±0.02 and 0.19±0.02 nmol min^{-1} in SS, for PM_{10} and $PM_{2.5}$ particles, respectively. Likely because suggests this assay was mainly associated with redox active species accumulated in the fine fraction. Otherwise, the AA assay exhibited a clear particle-size dependence, as $OP^{AA}{}_V$ responses were significantly higher for PM_{10} than for $PM_{2.5}$, i.e., 0.35±0.06 vs. 0.21±0.03 nmol min^{-1} m^{-3} in AW and 0.23±0.04 vs. 0.09±0.01 in SS (Table 2, bold values). This suggest that AA depletion is more affected by species present in coarse particles, especially to those generated by vehicular traffic, such as brake abrasion and re-suspended dust (Simonetti et al., 2018).

Concerning association of $OP^{DTT}{}_V$ and $OP^{AA}{}_V$ responses with PM_{10} components, data in Table 3 show that in AW both responses were significantly correlated with K^+, Ba, Cd, Fe, OC, and EC, which are markers of the "mixed anthropogenic" source, as found for $PM_{2.5}$ particles. In addition, OP^{AA}v responses were also significantly correlated with metals − Cr, Cu, Mn, V − and some organic compounds − MS^-, acetate, glycolate, propionate, formate, and pyruvate − that are components of the "heavy oils/secondary marine" source. (Table 1).

In SS, the association of OP_V responses with chemical components significantly varied with both the OP assay and PM fraction, as shown in Table 3, because of the changes with seasons of the pollution source contributions.

In PM_{10}, the OP^{DTT}v responses were correlated with NH_4^+, Cu, OC, EC, oxalate, and glycolate, in SS. These species were mainly associated with the biomass-burning component of the "mixed anthropogenic" source. Note that in SS the Mediterranean basin is a worldwide wildfire hotspot due to the occurrence of a huge number of wildfires. The PM_{10} OP^{DTT}v response was also associated in SS with the "sulphate" source of which NH_4^+ is a maker.

Otherwise, the PM_{10} OP^{AA}v responses were correlated with more species, namely NH_4^+, K^+, Ca^{2+}, SO_4^{2-}, MS^-, Mn, Ni, P, Ti, V, oxalate, and glycolate. The results of the PMF model showed that NH_4^+ and SO_4^{2-} were the dominant species of the "sulphate" source, V, Ni and MS^- were the main components of the "heavy oil/secondary marine" source, and Ca^{2+}, Mn, and Ti contributed to the "soil dust" source. Therefore, the PM_{10} OP^{AA}v responses were likely associated with the above-mentioned sources, whose contribution has almost doubled from AW to SS (Table S1). The negligible correlation of the OP^{AA}v responses with OC and EC was likely responsible for the significant OP^{AA}v decrease from 0.35±0.06 to 0.23±0.04 nmol min^{-1} m^{-3} from AW to SS (Table 2), being OC and EC the main species contributing to the PM_{10} mass (Figure 2a-b).

3.5.1 Regression analysis of the OP^{DTT} and OP^{AA} responses with individual species

To further highlight the sensitivity of the two OP assays to various PM components, regression analysis was applied to describe OP^{DTT}_V and OP^{AA}_V responses as a function of the chemical species. Linear regressions were computed for species in the $PM_{2.5}$ and PM_{10} samples for AW and SS data, separately. Among the obtained equations, the parameters of those of the most abundant and/or well correlated ($R^2 \geq 0.4$) components are reported in Table 4 (intercept, slope, linear correlation coefficient, R^2, and chi-square (χ^2) values to test goodness of the fit). Also multi-linear regressions were computed by including two or three chemical species: the best obtained results are reported in Table S4a (OP^{AA}_V) and S4b (OP^{DTT}_V) of SI, for AW and SS and for $PM_{2.5}$ and PM_{10} particles, respectively. In general, we can observe that the inclusion of two or more variables did not significantly improve the fitting goodness, measured by χ^2 value, in comparison with simple linear model. Therefore, the results of the linear regressions will be discussed in the following.

Overall, in AW, similar regressions were computed for the OP^{DTT}_V and OP^{AA}_V responses with OC, EC, POC, K^+ and Fe in both fractions. In particular, close slopes of the regression lines were computed, as a measure of the assay sensitivity to the investigated species (Table 4). An exception is K^+ in PM_{10}, as the slope of the OP^{AA}_V regression line is nearly 1.5 greater than that of OP^{DTT}_V (0.45±0.15 and 0.31±0.09 nmol min^{-1} μg^{-1}, respectively). This likely explained the higher OP^{AA}_V than OP^{DTT}_V responses measured in PM_{10} samples (Table 2).

By comparing the different particle size, we can observe that the sensitivity of the OP^{AA}_V responses toward POC, EC, K^+, Fe, and Cu decreases from PM_{10} to $PM_{2.5}$ particles in AW (Table 4). This is particularly marked for Cu, as the line slope is three times higher for PM_{10} (31±6 nmol min^{-1} μg^{-1}) than for $PM_{2.5}$ (10±3 nmol min^{-1} μg^{-1}). Furthermore, the Cu and Fe concentrations are nearly double in PM_{10} compared with $PM_{2.5}$. These results clearly account for the higher OP^{AA}_V response in PM_{10} than in PM2.5, besides indicating that the transition metals, especially Cu, significantly driven of OP^{AA}_V responses. Both reasons motivate the higher sensitivity of AA assay to coarse particle. Otherwise, the OP^{DTT}_V responses display higher sensitivity towards EC, POC and K^+ in $PM_{2.5}$, that have similar concentrations in both fractions (Table S1 of SI), supporting the finding that the DTT assay was more sensitive to PM2.5 than to PM10 particles (Table 2).

In SS, the OP^{AA}_V and OP^{DTT}_V values were roughly correlated ($R^2 \geq 0.4$) with POC, EC and SO_4^{2-} mass concentration for PM_{10} (Table 4). In these samples, SO_4^{2-} and OC were the most abundant redox active species, contributing on average by 14 and 22% to the PM_{10} mass (Figure 1d). Consequently, the OP^{DTT}_V and OP^{AA}_V responses may significantly vary day-by-day depending on the amount of SO_4^{2-} and/or OC in the tested PM_{10} sample, as shown in the study cases described in the following. For $PM_{2.5}$, both OP^{AA}_V and OP^{DTT}_V responses showed significant association with

POC and EC mass concentrations, with similar sensitivity of the two assays, i.e., ~ 0.05 nmol min^{-1} μg^{-1} for POC and ~ 0.10 nmol min^{-1} μg^{-1} for EC (Table 4).

In conclusion, the contrasts between the AA and DTT assay responses were likely associated with the different sensitivity of both assays towards specific emission sources, such as "sulphate", "heavy oil/secondary marine" and "soil dust" sources. This is in agreement with results found by other Authors, i.e., Calzolai et al., 2015; Jaafar et al., 2014; Shirmohammadi et al., 2017; Styszko et al., 2017; Verma, et al., 2015; Waked et al., 2014; Weber et al., 2018.

3.6. OP^{DTT}_V and OP^{AA}_V responses on selected monitoring days

The data of selected monitoring days were investigated in detail to relate the contrasts between the OP^{DTT}_V and OP^{AA}_V responses in $PM_{2.5}$ and PM_{10} samples with the change of the mass concentration of specific chemical species.

3.6.1. Study cases: 20 December 2014 and 11March 2015

The days 20 December 2014 and 11 March 2015 showed a different pattern of the OP^{AA}_V and OP^{DTT}_V values (Figure 2a-c). In fact, on 20 December 2014 the PM_{10} OP^{AA}_V reached the highest value (0.68 nmol min^{-1} m^{-3}), while the $PM_{2.5}$ OP^{AA}_V value (0.19 nmol min^{-1} m^{-3}) was smaller than the mean AW value (0.21 nmol min^{-1} m^{-3}). Otherwise, on 11 March 2015 the OP^{AA}_V values were rather similar for both size fractions (close to 0.20 nmol min^{-1} m^{-3}, Figure 2a). Concerning OP^{DTT}_V, the PM_{10} value was 0.37 nmol min^{-1} m^{-3} on 20 December and 0.25 nmol min^{-1} m^{-3} on 11 March, while the $PM_{2.5}$ value was 0.33 nmol min^{-1} m^{-3} and 0.27 nmol min^{-1} m^{-3}, respectively (Figure 2c).

The PM mass concentration was very similar in the two days, i.e., 26 and 25 $\mu g/m^3$ for $PM_{2.5}$ and 34 and 33 $\mu g/m^3$ for PM_{10} on 20 December and 11 March, respectively (Figure 2e). Therefore, the above outlined contrasts resulting from Figures 1a and 1c cannot be ascribed to differences in mass concentrations, but have to be searched in the different PM composition. The mass concentration of the main redox active species on 20 December (light grey bars) and 11 March (dark grey bars) are reported in Figure 3 for $PM_{2.5}$ (a) and PM_{10} (b) samples. More specifically, the left side axis of Figure 3 provides the mass concentration of the dominant chemical components, i.e., NH_4^+, K^+, NO_3^-, SO_4^{2-}, OC and EC, being their respective mass percentage ≥ 1% in the PM_{10} fraction (Table S1 of SI). The right side axis refers to the species characterized by a mass percentage <1% (MS^-, Ba, Cd, Cr, Cu, Fe, Mn, P, V, Zn, acetate, glycolate, propionate, formate, pyruvate), reported in light grey axis. The OC and EC mass concentrations reached one of the highest values on 20

December, while their mass was almost halved on 11 March. More specifically, OC and EC accounted for 53% and 27% of the PM_{10} mass and for 68% and 36 % of the $PM_{2.5}$ mass on 20 December and 11 March 2015, respectively. Therefore, we can infer that the high contrast between the PM_{10} $OP^{DTT}{}_V$ and $OP^{AA}{}_V$ values on 20 December was mainly due to the faster rate of change of the $OP^{AA}{}_V$ with the OC and EC mass concentrations than the $OP^{DTT}{}_V$ (Table 4). The contrast between the two assay responses decreases on 11 March, likely because of the remarkable decrease of the OC and EC mass contribution to the PM_{10} mass. Note also that the contribution of SOC particles was greater on 11 March than on 20 December, as indicated by the OC/EC mass ratio, which is 3.1 and 2.4 on 11 March and 20 December, respectively. Consequently, the significant decrease of the POC concentration on 11 March contributed to the above result, being the POC particles the main redox active species (Tables 3 and 4). The change in the PM chemical composition on the selected days can be explained by investigating the main airflows at the study site by using the HYSPLIT model (Draxler and Hess 1998). The 4-day HYSPLIT back trajectories that reached the study site at 12:00 UTC of 20 December (Figure 4a-b) show that the air masses associated with the 0.27 and 0.5 km arrival-height back trajectories came from the Central Mediterranean Sea and anthropogenic polluted areas in southern Italy. Conversely, on 11 March, back trajectories crossed Eastern Europe and therefore they likely transported aged carbonaceous particles or SOC enriched particles to the study site (Figure 4c-d).

3.6.2. Study Cases: 7 May 2015 and 29 July 2015

In SS period, an opposing trend of the $OP^{AA}{}_V$ and $OP^{DTT}{}_V$ values was observed in the days 7 May and 29 July (Figure 2b-d). On 7 May, $OP^{AA}{}_V$ reached one of its highest values (0.66 nmol min^{-1} m^{-3}) in PM_{10}, while it was more than 4 times smaller in $PM_{2.5}$ (0.16 nmol min^{-1} m^{-3}, Figure 2b). In the same day, $OP^{DTT}{}_V$ showed similar responses for both PM_{10} and $PM_{2.5}$ samples, i.e., close to their SS mean value. The PM_{10} ($PM_{2.5}$) mass concentration was equal to 41 (31) and 44 (34) µg/m^3 on 7 May and 29 July 2015, respectively (Figure 2f). This pattern can be related to the variation in the mass concentration of the main redox active species, as reported in Figure 5 for (a) $PM_{2.5}$ and (b) PM_{10} on 7 May (light grey bars) and 29 July (dark grey bars). On 7 May, the SO_4^{2-} mass concentration reached one of the highest values, i.e., 5.5 and 5.3 µg/m^3 in PM_{10} and $PM_{2.5}$, respectively. For PM_{10}, the significant association of $OP^{AA}{}_V$ with SO_4^{2-} (Table 4), may likely accounts for the difference between the PM_{10} $OP^{DTT}{}_V$ and $OP^{AA}{}_V$ values on 7 May (Figure 2b and 2d).

On 29 July 2015, the $OP^{AA}{}_V$ and $OP^{DTT}{}_V$ value was 0.08 and 0.29 nmol min^{-1} m^{-3}, respectively (Figures 2b and 2d). In this day, the SO_4^{2-} and OC mass concentration was equal to 3.6 and 8.0 µg

m^{-3}, respectively, in the PM_{10} sample (Figure 5b). The low SO_4^{2-} and high OC mass concentrations, respectively, have likely been responsible for the observed differences between the $OP^{AA}{}_V$ and $OP^{DTT}{}_V$ values. Concerning $OP^{DTT}{}_V$, similar responses were measured in $PM_{2.5}$ and PM_{10} samples. In contrast, the $OP^{AA}{}_V$ value was nearly twice larger in $PM_{2.5}$ than in PM_{10}, likely because of the higher $OP^{AA}{}_V$ sensitivity toward OC in $PM_{2.5}$ than that in PM_{10}.

Figure 6a-b shows that the 4-day HYSPLIT back trajectories crossed north-western Africa and the Mediterranean before reaching the study site at 12:00 UTC of 7 May, 2015. Therefore, the rather high mass concentrations of SO_4^{2-} and oxalate, respectively, are likely due to the prevalent stagnant conditions occurring in SS over the Mediterranean basin (e.g. Calzolai et al., 2015) and the enhanced photochemistry, which favours the formation of secondary aerosols. Moreover, the rather high Fe mass concentration monitored on 7 May indicates that they have likely been responsible for the transport of dust particles at the study site, according to Perrone et al. (2016). In contrast, the 4-day HYSPLIT back trajectories that reached the study site at 12:00 UTC of 29 May, 2015 came from the Atlantic Sea and crossed France and south western Italy before reaching the study site (Figure 6c-d).

4. Summary and Conclusion

In summary, we investigated the impact of size-distribution and chemical composition on OP^{DTT} and OP^{AA} responses of $PM_{2.5}$ and PM_{10} samples. We could identify specific contribution of the various chemical species and/or the pollution sources, because of the peculiarity of the study site, which is strongly impacted by long-range-transported particles from different sources, and the monitoring campaign duration all over the year. In addition, the comparison between the DTT and AA responses clearly highlighted that the two assays contrast in sensibility towards individual redox active species/sources.

We observed that in AW, the $OP^{DTT}{}_V$ and $OP^{AA}{}_V$ responses were associated with the "mixed anthropogenic" source in both $PM_{2.5}$ and PM_{10} particles. In addition, the PM_{10} OP^{AA}v responses were associated with the "heavy oils/secondary marine" source.

During SS, in $PM_{2.5}$, the ROS activity was associated with the "mixed anthropogenic" and the "reacted dust" sources. In PM_{10}, the OP^{DTT}v responses were mainly associated with the biomass-burning component of the "mixed anthropogenic" source, while the OP^{AA}v responses were likely driven by the "sulphate", "heavy oil/secondary marine", and "soil dust" sources.

Therefore, the variation of the $OP^{DTT}{}_V$ and $OP^{AA}{}_V$ responses with season can be explained by combining seasonal changing of $PM_{2.5}$ and PM_{10} chemical composition with the different sensitivity

of the DTT and AA assays to the various redox-active species. Overall, the DTT assay was more sensitive to species generated by combustion processes, mostly belonging to the fine mode particles. This last finding merits further investigation, also because of the increasing relevance of this source that has been recorded during the last years. Conversely, the AA assay was particularly sensitive to metals in PM_{10} particles, mainly generated by vehicular traffic, such as brake abrasion and re-suspended road dust.

Therefore, the results of this study should be considered helpful to design regulatory strategies toward establishing more effective and source-specific regulations for mitigating PM toxicity. Such policies could focus on reducing PM emissions from vehicular traffic and biomass burning. In addition, the chemical specificity observed for DTT and AA assays emphasizes the need of a standardized approach for the future studies on epidemiology or toxicology of the PM.

Acknowledgments

S. Romano has carried out this work with the support of a postdoctoral fellowship from the Consorzio Nazionale Interuniversitario per le Scienze Fisiche della Materia (CNISM). The financial support of EARLINET as part of the ACTRIS Research Infrastructure Project by the European Union's Horizon 2020 research and innovation programme under grant agreement no. 654109 and 739530 (previously under grant agreement no. 262254) in the 7th Framework Programme (FP7/2007-2013) is gratefully acknowledged. S. Becagli and R. Traversi are acknowledged for the ion and metal analyses on PM samples. The NOAA Air Resources Laboratory is kindly acknowledged for the provision of the HYSPLIT back trajectories.

527 **References**

528

529 Bardouki, H., Liakakou, H., Economou, C., Sciare, J., Smolík, J., Ždímal, V., Eleftheriadis, K.,
530 Lazaridis, M., Dye, C., Mihalopoulos, N., 2003. Chemical composition of size-resolved
531 atmospheric aerosols in the eastern Mediterranean during summer and winter. Atmos. Environ. 37,
532 195-208.
533 Bates, J.T., Weber, R.J., Abrams, J., Verma, V., Fang, T., Klein, M., Strickland, M.J., Sarnat, S.E.,
534 Chang, H.H., Mulholland, J.A., Tolbert, P.E., Russell, A.G., 2015. Reactive oxygen species
535 generation linked to sources of atmospheric particulate matter and cardiorespiratory effects.
536 Environ. Sci. Technol. 49, 13605-13612.
537 Becagli, S., Anello, F., Bommarito, C., Cassola, F., Calzolai, G., Di Iorio, T., di Sarra, A., Gómez-
538 Amo, J.-L-., Lucarelli, F., Marconi, M., Meloni, D., Monteleone, F., Nava, S., Pace, G., Severi, M.,
539 Sferlazzo, D.M., Traversi, R., Udisti, R., 2017. Constraining the ship contribution to the aerosol of
540 the central Mediterranean. Atmos. Chem. Phys. 17, 2067-2084.
541 Boogaard, H., Janssen, N.A.H., Fischer, P.H., Kos, G.P.A., Weijers, E.P., Cassee, F.R., van der
542 Zee, S.C., de Hartog, J.J., Brunekreef, B., Hoek, G., 2012. Contrasts in oxidative potential and other
543 particulate matter characteristics collected near major streets and background locations. Environ.
544 Health Perspect. 120, 185-191.
545 Calas, A., Uzu, G., Kelly, F.J., Houdier, S., Martins, J.M.F., Thomas, F., Molton, F., Charron, A.,
546 Dunster, C., Oliete, A., Jacob, V., Besombes, J.L., Chevrier, F., Jaffrezo, J.L., 2018. Comparison
547 between five acellular oxidative potential measurement assays performed with detailed chemistry
548 on PM_{10} samples from the city of Chamonix (France). Atmos. Chem. Phys. 18, 7863-7875.
549 Calzolai, G., Nava, S., Lucarelli, F., Chiari, M., Giannoni, M., Becagli, S., Traversi, R., Marconi,
550 M., Frosini, D., Severi, M., Udisti, R., di Sarra, A., Pace, G., Meloni, D., Bommarito, C.,
551 Monteleone, F., Anello, F., Sferlazzo, D.M., 2015. Characterization of PM_{10} sources in the central
552 Mediterranean. Atmos. Chem. Phys. 15, 13939-13955.
553 Cavalli, F., Viana, M., Yttri, K.E., Genberg, J., Putaud, J., 2010. Toward a standardised thermal-
554 optical protocol for measuring atmospheric organic and elemental carbon: the EUSAAR protocol.
555 Atmos. Meas. Tech. 3, 79-89.
556 CEC (Commission of the European Communities), 2008. Directive 2008/50/EC of the European
557 Parliament and of the Council of 21 May 2008 on ambient air quality and cleaner air for Europe.
558 Official Journal of the European Union, L152, 1-44.
559 Chalupa, D.C., Morrow, P.E., Oberdorster, G., Utell, M.J., Frampton, M.W., 2004. Ultrafine
560 particle deposition in subjects with asthma. Environ. Health Per. 112, 879-882.

561 Charrier, J.G. and Anastasio, C., 2012. On dithiothreitol (DTT) as a measure of oxidative potential
562 for ambient particles: evidence for the importance of soluble transition metals. Atmos. Chem. Phys.
563 12, 11317-11350.
564 Chirizzi, D., Cesari, D., Guascito, M.R., Dinoi, A., Giotta, L., Donateo, A., Contini, D., 2017.
565 Influence of Saharan dust outbreaks and carbon content on oxidative potential of water-soluble
566 fractions of $PM_{2.5}$ and PM_{10}. Atmos. Environ. 163, 1-8.
567 Cho, A.K., Sioutas, C., Miguel, A.H., Kumagai, Y., Schmitz, D.A., Singh, M., Eiguren-Fernandez,
568 A., Froines, J.R., 2005. Redox activity of airborne particulate matter at different sites in the Los
569 Angeles Basin. Environ. Res. 99, 40-47.
570 Crobeddu, B., Aragao-Santiago, L., Bui, L.C., Boland, S., Baeza Squiban, A., 2017. Oxidative
571 potential of particulate matter 2.5 as predictive indicator of cellular stress. Environ. Pollut. 230,
572 125-133.
573 Daher, N., Saliba, N.A., Shihadeh, A.L., Jaafar, M., Baalbaki, R., Shafer, M.M., Schauer, J.J.,
574 Sioutas, C., 2014. Oxidative potential and chemical speciation of size-resolved particulate matter
575 (PM) at near-freeway and urban background sites in the greater Beirut area. Sci. Total Environ.
576 470-471, 417-426.
577 Draxler, R.R., Hess, G.D., 1998. An overview of the HYSPLIT_4 modeling system of trajectories,
578 dispersion, and deposition. Australian Met. Mag. 47, 295-308.
579 Fang, T., Verma, V., Bates, J.T., Abrams, J., Klein, M., Strickland, M.J., Sarnat, S.E., Chang, H.H.,
580 Mulholland, J.A., Tolbert, P.E., Russell, A.G., Weber, R.J., 2016. Oxidative potential of ambient
581 water-soluble $PM_{2,5}$ in the southeastern United States: contrasts in sources and health associations
582 between ascorbic acid (AA) and dithiothreitol (DTT) assays. Atmos. Chem. Phys. 16, 3865-3879.
583 Fang, T., Zeng, L., Gao, D., Verma, V., Stefaniak, A.B., Weber, R.J., 2017. Ambient Size
584 Distributions and Lung Deposition of Aerosol Dithiothreitol-Measured Oxidative Potential:
585 Contrast between Soluble and Insoluble Particles. Environ. Sci. Technol. 51, 6802-6811.
586 Hasheminassab, S., Daher, N., Saffari, A., Wang, D., Ostro, B.D., Sioutas, C., 2014. Spatial and
587 temporal variability of sources of ambient fine particulate matter ($PM_{2.5}$) in California. Atmos.
588 Chem. Phys. 14, 12085-12097.
589 Jaafar, M., Baalbaki, R., Mrad, R., Daher, N., Shihadeh, A., Sioutas, C., Saliba, N.A., 2014. Dust
590 episodes in Beirut and their effect on the chemical composition of coarse and fine particulate
591 matter. Sci. Total Environ. 496, 75-83.
592 Janssen, N.A.H., Yang, A., Strak, M., Steenhof, M., Hellack, B., Gerlofs-Nijland, M.E., Kuhlbusch,
593 T., Kelly, F., Harrison, R., Brunekreef, B., Hoek, G., Cassee, F., 2014. Oxidative potential of

particulate matter collected at sites with different source characteristics. Sci. Tot. Environ. 472, 572-581.

Janssen, N.A.H., Strak, M., Yang, A., Hellack, B., Kelly, F.J., Kuhlbusch, T.A.J., Harrison, R.M., Brunekreef, B., Cassee, F.R., Steenhof, M., Hoek, G., 2015. Associations between three specific a-cellular measures of the oxidative potential of particulate matter and markers of acute airway and nasal inflammation in healthy volunteers. Occup. Environ. Med. 72, 49-56.

Kelly, F.J., 2003. Oxidative stress: its role in air pollution and adverse health effects. Occup. Environ. Med. 60, 612-616.

Lovett, C., Sowlat, M.H., Saliba, N.A., Shihadeh, A.L., Sioutas, C., 2018. Oxidative potential of ambient particulate matter in Beirut during Saharan and Arabian dust events. Atmos. Environ. 188, 34-42.

Lyu, Y., Guo, H., Cheng, T., Li, X., 2018. Particle Size Distributions of Oxidative Potential of Lung-Deposited Particles: Assessing Contributions from Quinones and Water-Soluble Metals. Environ. Sci. Technol. 52, 6592-6600.

Mittal, M., Siddiqui, M.R., Tran, K., Reddy, S.P., Malik, A.B., 2014. Reactive Oxygen Species in Inflammation and Tissue Injury. Antioxid. Redox Signal 20, 1126-1167.

Moreno, T., Kelly, F.J., Dunster, C., Oliete, A., Martins, V., Reche, C., Minguillòn, M.C., Amato, F., Capdevila, M., de Miguel, E., Querol, X., 2017. Oxidative potential of subway $PM_{2.5}$. Atmos. Environ. 148, 230-238.

Mudway, I.S., Stenfors, N., Duggan, S.T., Roxborough, H., Zielinski, H., Marklund, S.L., Blomberg, A., Frew, A.J., Sandström, T., Kelly, F. J., 2004. An in vitro and in vivo investigation of the effects of diesel exhaust on human airway lining fluid antioxidants. Arch. Biochem. Biophys., 423, 200-212.

Mugica, V., Ortiz, E., Molina, L., De Vizcaya-Ruiz, A., Nebot, A., Quintana, R., Aguilar, J., Alcántara, E., 2009. PM composition and source reconciliation in Mexico City. Atmos. Environ. 43, 5068-5074.

Perez, N., Pey, J., Castillo, S., Viana, M., Alastuey, A., Querol, X., 2008. Interpretation of the variability of levels of regional background aerosols in the Western Mediterranean. Sci. Tot. Environ. 407, 527-540.

Pant, P., Baker, S.J., Shukla, A., Maikawa, C., Godri Pollitt K.J., Harrison, R.M., 2015. The PM_{10} fraction of road dust in the UK and India: Characterization, source profiles and oxidative potential. Sci. Tot. Environ. 530-531, 445-452.

626 Perrone, M.R., Becagli, S., Garcia Orza, J.A., Vecchi, R., Dinoi, A., Udisti, R., Cabello, M., 2013.
627 The impact of long-range-transport on PM_1 and $PM_{2.5}$ at a Central Mediterranean site. Atmos.
628 Environ. 71, 176-186.
629 Perrone, M.R., Dinoi, A., Becagli, S., Udisti, R., 2014a. Chemical composition of PM_1 and $PM_{2.5}$ at
630 a suburban site in southern Italy. Intern. J. Environ. Anal. Chem. 94, 127-150.
631 Perrone, M.R., Romano, S., Orza, J.A.G., 2014b. Particle optical properties at a Central
632 Mediterranean site: Impact of advection routes and local meteorology. Atmos. Res. 145-146, 152-
633 167.
634 Perrone, M.R., Genga, A., Siciliano, M., Siciliano, T., Paladini, F., Burlizzi, P., 2016. Saharan dust
635 impact on the chemical composition of PM_{10} and PM_1 samples over south-eastern Italy. Arabian J.
636 Geosc. 9 (2), article 127.
637 Perrone, M.R. and Romano, S., 2018. Relationship between the planetary boundary layer height and
638 the particle scattering coefficient at the surface. Atmos. Res. 213, 57-69.
639 Perrone, M.R., Vecchi, R., Romano S., Becagli, S., Traversi, R., Paladini, F., 2019. Weekly cycle
640 assessment of PM mass concentrations and sources, and impacts on temperature and wind speed in
641 Southern Italy. Atmos Res. 218, 129–144.
642 Pietrogrande, M.C., Perrone, M.R., Manarini, F., Romano, S., Udisti, R., Becagli, S., 2018a. PM_{10}
643 oxidative potential at a Central Mediterranean Site: Association with chemical composition and
644 meteorological parameters. Atmos. Environ. 188, 97-111.
645 Pietrogrande, M.C., Dalpiaz, C., Dell'Anna, R., Lazzeri, P., Manarini, F., Visentin, M., Tonidandel,
646 G. 2018b. Chemical composition and oxidative potential of atmospheric coarse particles at an
647 industrial and urban background site in the alpine region of northern Italy. Atmos. Environ. 191,
648 340-350.
649 Pio, C., Cerqueira, M., Harrison, R.M., Nunes, T., Mirante, F., Alves, C., Oliveira, C., Sanchez de
650 la Campa, A., Artíñano, B., Matos M., 2011. OC/EC ratio observations in Europe: re-thinking the
651 approach for apportionment between primary and secondary organic carbon. Atmos. Environ. 45,
652 6121-6132.
653 Poschl, U. and Shiraiwa, M., 2015. Multiphase Chemistry at the Atmosphere−Biosphere Interface
654 Influencing Climate and Public Health in the Anthropocene. Chem. Rev. 115, 4440-4475.
655 Querol, X., Alastuey, A., Moreno, T., Viana, M., Castillo, S., Pey, J., Rodríguez, S., Artiñano, B.,
656 Salvador, P., Sánchez, M., Garcia Dos Santos, S., Herce Garraleta, M.D., Fernandez-Patier, R.,
657 Moreno-Grau, S., Minguillón, M.C., Monfort, E., Sanz, M.J., Palomo-Marín, R., Pinilla-Gil, E.,
658 Cuevas, E., 2008. Spatial and temporal variations in airborne particulate matter (PM_{10} and $PM_{2.5}$)
659 across Spain 1999-2005. Atmos. Environ. 42, 3964-3979.

Reid, J.S., Koppmann, R., Eck, T.F., Eleuterio, D.P., 2005. A review of biomass burning emissions part II: intensive physical properties of biomass burning particles. Atmos. Chem. Phys. 5, 799-825.

Samara, C., 2017. On the Redox Activity of Urban Aerosol Particles: Implications for Size Distribution and Relationships with Organic Aerosol Components. Atmos. 8, 205.

Sandrini S., Fuzzi, S., Piazzalunga, A., Prati, P., Bonasoni, Cavalli, F., Bove M.C., Calvello, M., Cappelletti, D., Colombi, C., Contini, D., de Gennaro, G., Di Gilio, A., Fermo, P., Ferrero, L., Gianelle, V., Giugliano, M., Ielpo, P., Lonati, G., Marinoni, A., Massabò, D., Molteni, U., Moroni, B., Pavese, G., Perrino, C., Perrone, M.G., Perrone, M.R., Putaud, J.P., Sargolini, T., Vecchi, R., Gilardoni, S., 2014. Spatial and seasonal variability of carbonaceous aerosol across Italy. Atmos. Environ. 99, 587-598.

Shafer, M.M., Hemming, J.D., Antkiewicz, D.S., Schauer, J.J., 2016. Oxidative potential of size-fractionated atmospheric aerosol in urban and rural sites across Europe. Faraday Discuss. 189, 381-405.

Shirmohammadi, F., Wang, D., Hasheminassab, S., Verma, V., Schauer, J.J., Shafer, M.M., Sioutas, C., 2017. Oxidative potential of on-road fine particulate matter ($PM_{2.5}$) measured on major freeways of Los Angeles, CA, and a 10-year comparison with earlier roadside studies. Atmos. Environ. 148, 102-114.

Shuster-Meiseles, T., Shafer, M.M., Heo J., Pardo, M., Antkiewicz D.S., Schauer, J.J., Rudich, A., Rudich, Y., 2016. ROS-generating/ARE-activating capacity of metals in roadway particulate matter deposited in urban environment. Environ. Res. 146, 252-262.

Simonetti, G., Conte, E., Perrino, C., Canepari, S., 2018. Oxidative potential of size-segregated PM in an urban and an industrial area of Italy. Atmos. Environ. 187, 292-300.

Szigeti, T., Dunster, C., Cattaneo, A., Cavallo, D., Spinazzè, A., Saraga, D.E., Sakellaris, I.A., de Kluizenaar, Y., Cornelissen, E.J.M., Hänninen, O., Peltonen, M., Calzolai, G., Lucarelli, F., Mandin, C., Bartzis, J.G., Záray, G., Kelly, F.J., 2016. Oxidative potential and chemical composition of PM2.5 in office buildings across Europe – The OFFICAIR study. Environ. Int. 92-93, 324-333.

Styszko, K., Samek, L., Szramowiat, K., Korzeniewska, A., Kubisty, K., Rakoczy-Lelek, R., Kistler, M., Giebl, A.K., 2017. Oxidative potential of PM_{10} and $PM_{2.5}$ collected at high air pollution site related to chemical composition: Krakow case study. Air Qual. Atmos. Health 10, 1123-1137.

Valko, M., Morris, H., Cronin, M.T, 2005. Metals, toxicity and oxidative stress. Curr. Med. Chem. 12, 1161-1208.

692 Venkatachari, P., Hopke, P.K., 2008. Development and Laboratory Testing of an Automated
693 Monitor for the Measurement of Atmospheric Particle-Bound Reactive Oxygen Species (ROS).
694 Aerosol Sci. Technol. 42, 629-635.
695 Verma, V., Fang, T., Xu, L., Peltier, R.E., Russel, A.G., Ng, N.L., Weber, R.J., 2015. Organic
696 Aerosols Associated with the Generation of Reactive Oxygen Species (ROS) by Water-Soluble
697 $PM_{2.5}$. Environ. Sci. Technol. 49, 4646-4656.
698 Visentin, M., Pagnoni, A., Sarti, E., Pietrogrande, M.C., 2016. Urban $PM_{2.5}$ oxidative potential:
699 Importance of chemical species and comparison of two spectrophotometric cell-free assays.
700 Environ. Pollut. 219, 72-79.
701 Waked, A., Favez, O., Alleman, L.Y., Piot, C., Petit, J.E., Delaunay, T., Verlinden, E., Golly, B.,
702 Besombes, J.L., Jaffrezo, J.L., Leoz-Garziandia, E., 2014. Source apportionment of PM_{10} in a north-
703 western Europe regional urban background site (Lens, France) using positive matrix factorization
704 and including primary biogenic emissions. Atmos. Chem. Phys. 14, 3325-3346.
705 Weber, S., Uzu, G., Calas, A., Chevrier, F., Besombes, J.L., Charron, A., Salameh, D., Jevzek, I.,
706 Movcnik, G., Jaffrezo, J.L., 2018. An apportionment method for the oxidative potential of
707 atmospheric particulate matter sources: application to a one-year study in Chamonix, France.
708 Atmos. Chem. Phys. 18, 9617-9629.
709 Yang, A., Jedynska, A., Hellack, B., Kooter, I., Hoek, G., Brunekreef, B., Kuhlbusch, T.A.J.,
710 Cassee, F.R., Janssen N.A.H., 2014. Measurement of the oxidative potential of $PM_{2.5}$ and its
711 constituents: the effect of extraction solvent and filter type. Atmos. Environ. 83, 35-42.
712 Zhang, Z., Gao, J., Zhang, L., Wang, H., Tao, J., Qiu, X., Chai, F., Li, Y., Wang, S., 2017.
713 Observations of biomass burning tracers in $PM_{2.5}$ at two megacities in North China during 2014
714 APEC summit. Atmos. Environ. 169, 54–64.
715

716 **Table 1.** Aerosol sources (and main markers) for PM2.5 and PM10 particles. The percentage
717 contribution of each source is also provided for AW (Autumn-Winter) and SS (Spring-Summer),
718 extracted from Perrone et al. (2019).

719

Source	PM2.5		PM10	
	AW (%)	**SS (%)**	**AW (%)**	**SS (%)**
Sulphate (SO_4^{2-}, NH_4^+, Pb)	17.5	46.1	13.2	28.8
Heavy Oils / Sec. Marine (V, Ni, Cr, MS^-)	0.1	0.5	0.4	2.1
Mixed Anthropogenic (EC, OC, K^+, Cu, Fe, Ba)	55.3	15.9	59.7	28.1
Soil Dust (Al, Ca^{2+}, Sr, Ti, Fe, Mn)	7.9	9.3	12.1	23.5
Reacted Dust (NO_3^-, SO_4^{2-})	2.9	11.7	6.4	12.5
Sea Salt (Na^+, Cl^-)	16.3	16.6	8.3	5.0

720

721

722 **Table 2.** Volume- (OP_V) and mass-normalized (OP_m) Oxidative Potential responses measured for
723 PM_{10} and $PM_{2.5}$ with DTT (OP^{DTT}) and AA assays (OP^{AA}): mean values and standard errors of the
724 mean (SEMs) computed for autumn-winter (AW, 15 days) and spring-summer (SS, 24 days) data,
725 separately. Values with significant ($p<0.05$) difference between the seasons are marked by * and
726 those with significant ($p<0.05$) differences between the PM_{10} and $PM_{2.5}$ fractions are reported in
727 **bold**.

728

Oxidative Potential	Autumn-Winter				Spring-Summer			
	PM_{10}		$PM_{2.5}$		PM_{10}		$PM_{2.5}$	
	Mean	SEM	Mean	SEM	Mean	SEM	Mean	SEM
OP^{AA}_V ($nmol^{AA}\ min^{-1}\ m^{-3}$)	**0.35**	0.06	**0.21***	0.03	**0.23**	0.04	**0.09***	0.01
OP^{DTT}_V ($nmol^{DTT}\ min^{-1}\ m^{-3}$)	0.24	0.04	0.29*	0.03	0.22	0.02	0.19*	0.02
OP^{AA}_m ($nmol^{AA}\ min^{-1}\ \mu g^{-1}$)	0.010	0.002	0.008*	0.001	**0.008**	0.001	**0.005***	0.001
OP^{DTT}_m ($nmol^{DTT}\ min^{-1}\ \mu g^{-1}$)	**0.007**	0.001	**0.011**	0.001	0.008	0.001	0.010	0.001

729

730

731 **Table 3.** Pearson correlation coefficients (r) between OP^{DTT}_V and OP^{AA}_V responses and chemical components in PM_{10} and $PM_{2.5}$ particles computed
732 for autumn-winter (AW, 15 days) and spring-summer (SS, 24 days) data, separately. Statistically significant correlations are marked by *** at p <
733 0.01 level, ** at p < 0.02 level, and * at p < 0.05 level.

Parameter	Autumn-Winter				Spring-Summer			
	PM_{10}		$PM_{2.5}$		PM_{10}		$PM_{2.5}$	
	OP^{AA}_V	OP^{DTT}_V	OP^{AA}_V	OP^{DTT}_V	OP^{AA}_V	OP^{DTT}_V	OP^{AA}_V	OP^{DTT}_V
PM_{10} OP^{AA}_V	**1.00**	0.50	**0.61****	**0.75*****	**1.00**	**0.45***	0.20	0.29
PM_{10} OP^{DTT}_V	0.50	**1.00**	**0.70*****	**0.65*****	**0.45***	**1.00**	**0.42***	**0.57*****
$PM_{2.5}$ OP^{AA}_V	**0.61****	**0.70*****	**1.00**	**0.91*****	0.20	**0.42***	**1.00**	**0.70*****
$PM_{2.5}$ OP^{DTT}_V	**0.75*****	**0.65*****	**0.91*****	**1.00**	**0.29**	**0.57*****	**0.70*****	**1.00**
PM_{10} mass	0.47	**0.70*****	**0.84*****	**0.81*****	0.24	0.30	**0.50*****	**0.72*****
$PM_{2.5}$ mass	0.46	**0.59****	**0.82*****	**0.79*****	0.18	0.24	**0.47****	**0.63*****
Na^+	**-0.64*****	-0.49	-0.32	-0.43	**-0.40***	-0.18	**0.41***	0.29
NH_4^+	-0.32	-0.05	-0.07	-0.05	**0.63*****	**0.43***	-0.25	0.00
K^+	**0.64*****	**0.70*****	**0.79*****	**0.73*****	**0.44***	0.25	0.19	0.26
Mg^{2+}	-0.41	-0.23	-0.06	-0.09	0.17	0.14	0.01	0.13
Ca^{2+}	0.18	0.32	0.23	0.27	**0.52*****	0.27	0.02	0.14
Cl^-	-0.46	-0.23	-0.14	-0.20	**-0.53*****	**-0.49****	0.08	-0.03
NO_3^-	0.13	0.46	**0.60****	**0.66*****	-0.00	0.39	**0.51*****	**0.45***
SO_4^{2-}	-0.36	-0.15	-0.05	-0.04	**0.71*****	0.34	-0.22	0.01
MS^-	**0.62*****	0.12	0.21	0.26	**0.52*****	0.00	-0.35	-0.05
Al	0.13	0.02	-0.01	0.04	0.37	-0.00	-0.06	0.20
Ba	**0.89*****	**0.57***	**0.67*****	**0.62*****	0.22	0.30	0.45	0.34
Cd	**0.67*****	**0.55***	**0.75*****	**0.73*****	-0.11	0.02	0.18	0.31
Ce	0.27	0.38	**0.53***	0.40	0.07	-0.18	-0.26	-0.14
Co	-0.06	0.22	0.28	0.32	-0.08	-0.32	0.09	-0.18
Cr	**0.61****	0.23	0.37	0.35	0.09	0.27	0.14	0.02
Cu	**0.84*****	0.50	**0.64*****	**0.56***	0.21	**0.52*****	**0.63*****	**0.47****
Fe	**0.76*****	**0.53***	**0.76*****	**0.80*****	0.38	0.26	0.17	0.34
La	0.19	0.22	0.24	0.10	0.21	-0.18	-0.38	-0.06
Mn	**0.57***	0.38	**0.58****	**0.66*****	**0.46****	0.13	0.15	0.32
Mo	0.19	0.21	-0.47	-0.44	0.14	-0.08	**-0.43***	-0.33
Ni	0.29	0.16	0.27	0.04	**0.48****	-0.08	-0.25	-0.10
P	0.17	0.29	**0.76*****	**0.72*****	**0.56*****	0.15	0.04	0.07
Pb	-0.28	0.00	0.49	0.44	0.16	0.14	0.34	0.29
Sr	-0.03	-0.15	0.24	0.18	0.34	-0.06	-0.05	0.18
Ti	0.17	0.06	0.14	0.21	**0.44***	0.07	0.06	-0.21
V	**0.63*****	0.42	**0.73*****	**0.77*****	**0.59*****	0.13	-0.21	0.02
Zn	-0.44	-0.43	0.64***	0.41	0.38	-0.13	-0.09	-0.03
OC	**0.65*****	**0.76*****	**0.83*****	**0.80*****	0.02	**0.52*****	**0.64*****	**0.65*****
EC	**0.71*****	**0.77*****	**0.86*****	**0.84*****	0.22	**0.63*****	**0.75*****	**0.73*****
POC	**0.71*****	**0.77*****	**0.86*****	**0.83*****	0.22	**0.62*****	**0.73*****	**0.71*****
SOC	-0.27	-0.04	-0.32	-0.39	-0.11	0.38	**0.40***	**0.43***
Oxalate	0.19	0.29	**0.55***	**0.52***	**0.53*****	**0.41***	0.25	0.39
Acetate	**0.66*****	0.35	**0.67*****	**0.58****	-0.06	-0.01	0.24	0.26
Glycolate	**0.58****	0.44	**0.60****	**0.59****	**0.41***	0.13	0.29	0.34
Propionate	**0.78*****	0.38	0.35	0.31	-0.00	**0.44***	-0.12	0.04
Formate	**0.65*****	0.37	0.37	0.33	0.36	0.03	0.28	0.23
Pyruvate	**0.63*****	0.19	-0.05	0.04	**-0.50*****	-0.05	-0.09	-0.36

734 **Table 4**. Parameters of the linear regression equations linking the OP^{AA}_V and OP^{DTT}_V responses with the tracer
735 concentrations measured in PM_{10} and $PM_{2.5}$ samples, in Autumn-Winter (AW, October-March, 15 samples) and in
736 Spring-Summer (SS, April-September, 24 samples). The squared correlation coefficient (R^2) and the chi-square (χ^2)
737 value provide a measure of the corresponding linear correlation and the goodness of the fit, respectively. Note that only
738 the linear regression lines related to chemical species significantly correlated with OP_V with a p-level < 0.01 have been
739 reported.
740

	OP^{AA}_V			OP^{DTT}_V		
Species	**Intercept** (nmol min^{-1} m^{-3})	**Slope** (nmol min^{-1} μg^{-1})	**R^2 (χ^2)**	**Intercept** (nmol min^{-1} m^{-3})	**Slope** (nmol min^{-1} μg^{-1})	**R^2 (χ^2)**
			PM_{10} AW			
EC	0.11±0.08	0.07±0.02	0.50 (0.31)	0.08±0.04	0.05±0.01	0.59 (0.11)
POC	0.11±0.09	0.03±0.01	0.50 (0.31)	0.08±0.04	0.02±0.01	0.59 (0.11)
K^+	0.10±0.09	0.45±0.15	0.41 (0.37)	0.08±0.05	0.31±0.09	0.49 (0.13)
Cu	0.02±0.07	31±6	0.71 (0.18)	-	-	-
Fe	0.03±0.05	1.7±0.4	0.58 (0.27)	-	-	-
			$PM_{2.5}$ AW			
EC	0.04±0.03	0.05±0.01	0.74 (0.06)	0.14±0.03	0.04±0.01	0.71 (0.06)
POC	0.04±0.04	0.025±0.004	0.74 (0.06)	0.14±0.05	0.022±0.004	0.69 (0.06)
K^+	0.04±0.04	0.30±0.07	0.62 (0.09)	0.14±0.04	0.25±0.06	0.53 (0.09)
NO_3^-	-	-	-	0.15±0.05	0.13±0.04	0.44 (0.11)
Cu	0.13±0.04	10±3	0.41 (0.13)	-	-	-
Fe	0.01±0.01	1.4±0.3	0.58 (0.11)	0.12±0.04	1.6±0.3	0.64 (0.07)
			PM_{10} SS			
EC	-	-	-	0.07±0.04	0.09±0.02	0.40 (0.13)
POC	-	-	-	0.07±0.04	0.04±0.01	0.38 (0.13)
Cu	-	-	-	0.09±0.04	18±7	0.27 (0.16)
Ca^{2+}	0.00±0.09	0.24±0.08	0.27 (0.67)	-	-	-
SO_4^{2-}	-0.11±0.08	0.09±0.02	0.71 (0.45)	-	-	-
			$PM_{2.5}$ SS			
EC	-0.03±0.03	0.08±0.02	0.56 (0.04)	0.03±0.02	0.10±0.01	0.53 (0.07)
POC	-0.03±0.02	0.04±0.01	0.53 (0.04)	0.03±0.03	0.05±0.01	0.50 (0.07)
NO_3^-	0.05±0.02	0.08±0.03	0.26 (0.07)	-	-	-
Cu	0.00±0.03	26±7	0.40 (0.06)	-	-	-

741
742

Figure captions

Figure 1. Mean mass percentage distribution of the tested chemical species for the PM2.5 samples collected in (a) AW (Autumn-Winter) and in (b) SS (Spring-Summer) and the PM10 samples collected in (c) AW and in (d) SS. Al, Ba, Cd, Ce, Co, Cr, Cu, Fe, La, Mn, Mo, Ni, P, Pb, Sr, Ti, V, and Zn are represented by Met. MS-, oxalate, acetate, glycolate, propionate, formate, and pyruvate are indicated by Oxi. The undetermined mass is denoted as UM.

Figure 2. Daily evolution of the volume-normalized OP_V values in $PM_{2.5}$ and PM_{10} particles (dark and light grey bars, respectively). Figures 1a and 1b: $OP^{AA}{}_V$ responses measured with DTT assay for Autumn-Winter (a) and Spring-Summer (b) periods; Figures 1c and 1d: $OP^{DTT}{}_V$ responses measured with AA assay for Autumn-Winter (c) and Spring-Summer (d) periods; Figures 1e and 1f: temporal evolution of the $PM_{2.5}$ and PM_{10} mass concentration in Autumn-Winter (e) and Spring-Summer (f).

Figure 3. Mass concentration of the main redox active species measured on 20 December 2014 and 11 March 2015 (light and dark grey bars, respectively) in $PM_{2.5}$ (a) and PM_{10} particles. The chemical compounds marked in black and in grey are referred to the left and right y-axis, respectively. AC, GL, PR, FO, and PY represent the acetate, glycolate, propionate, formate, and pyruvate mass concentration.

Figure 4. Four-day analytical back trajectories reaching the monitoring site (Lecce, Italy) at 270 (red), 500 (blue), and 1000 m (green) above the ground level, at 12:00 UTC of 20 December 2014 (a) and 11 March 2015 (c). Figures 3b and 3d: altitude of each back trajectory as a function of time on 20 December 2014 (a) and 11 March 2015 (c), respectively.

Figure 5. Mass concentration of the main redox active species measured on 7 May and 29 July 2015 (light and dark grey bars, respectively) in $PM_{2.5}$ (a) and PM_{10} particles. The chemical compounds marked in black and in grey are referred to the left and right y-axis, respectively. AC, GL, PR, FO, and PY represent the acetate, glycolate, propionate, formate, and pyruvate mass concentration.

Figure 6. Four-day analytical back trajectories reaching the monitoring site (Lecce, Italy) at 270 (red), 500 (blue), and 1000 m (green) above the ground level, at 12:00 UTC of 7 May (a) and 29

July 2015 (c). Figures 5b and 5d: altitude of each back trajectory as a function of time on 7 May (a) and 29 July 2015 (c), respectively.

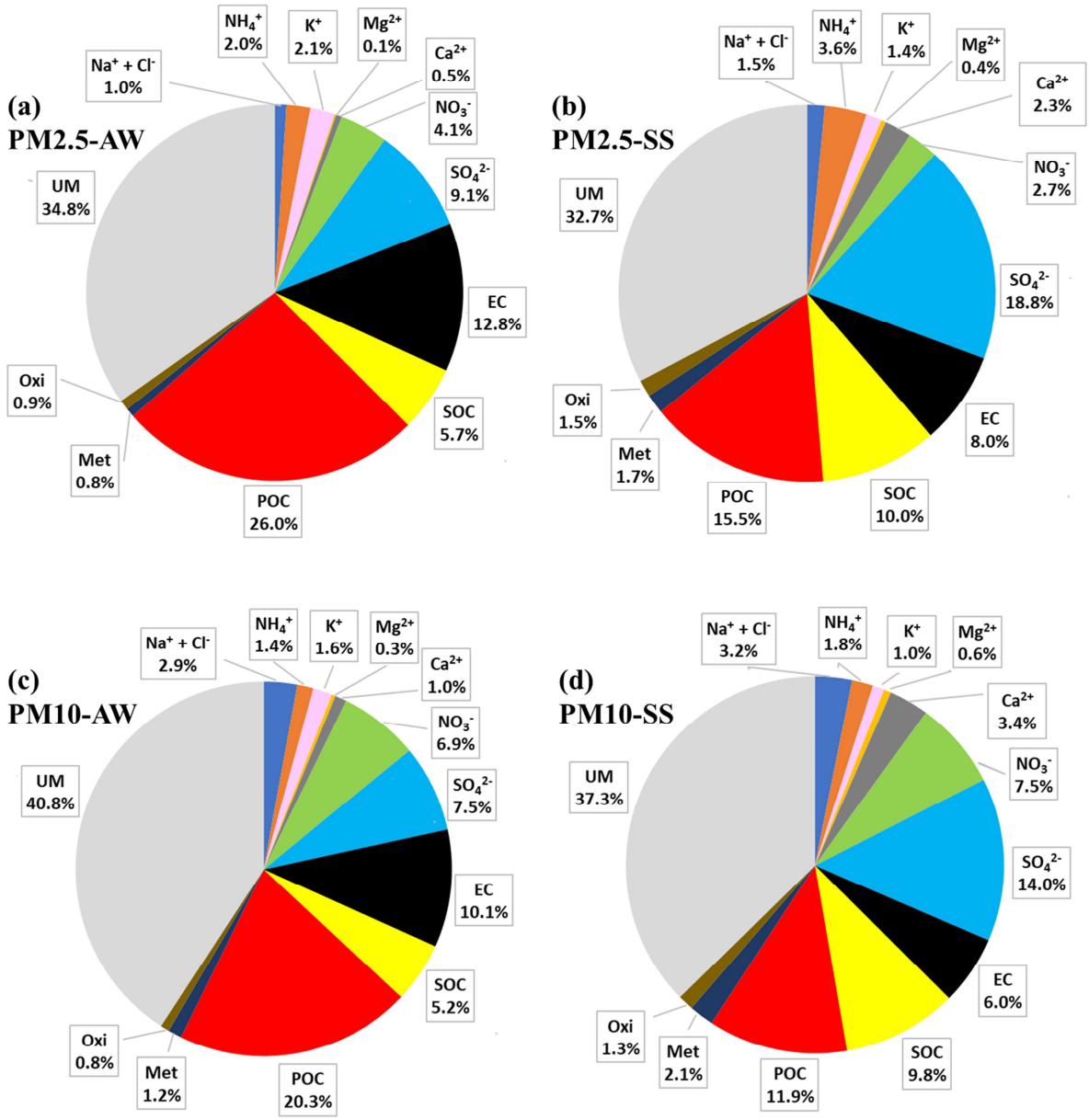

Figure 1. Mean mass percentage distribution of the tested chemical species for the PM2.5 samples collected in (a) AW (Autumn-Winter) and in (b) SS (Spring-Summer) and the PM10 samples collected in (c) AW and in (d) SS. Al, Ba, Cd, Ce, Co, Cr, Cu, Fe, La, Mn, Mo, Ni, P, Pb, Sr, Ti, V, and Zn are represented by Met. MS-, oxalate, acetate, glycolate, propionate, formate, and pyruvate are indicated by Oxi. The undetermined mass is denoted as UM.

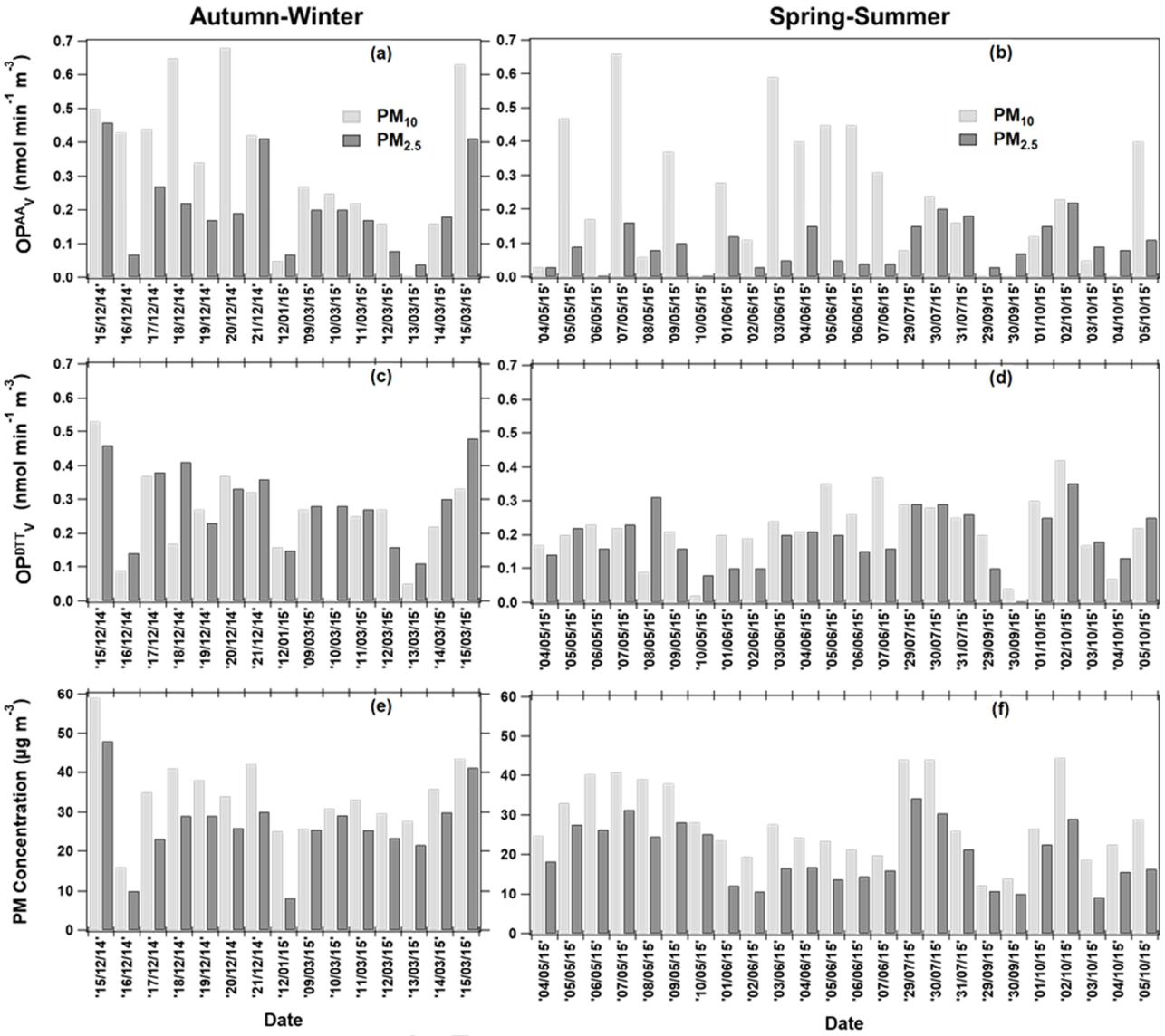

Figure 2. Temporal evolution of the volume-normalized oxidative potential (OP_V) values measured with the AA assay for (a) Autumn-Winter and (b) Spring-Summer, and the DTT assays for (c) Autumn-Winter and (d) Spring-Summer, for PM_{10} and $PM_{2.5}$ samples (light and dark grey bars, respectively). The temporal evolution of the PM_{10} and $PM_{2.5}$ concentration (light and dark grey bars, respectively) is also reported in (e) for Autumn-Winter and in (f) for Spring-Summer.

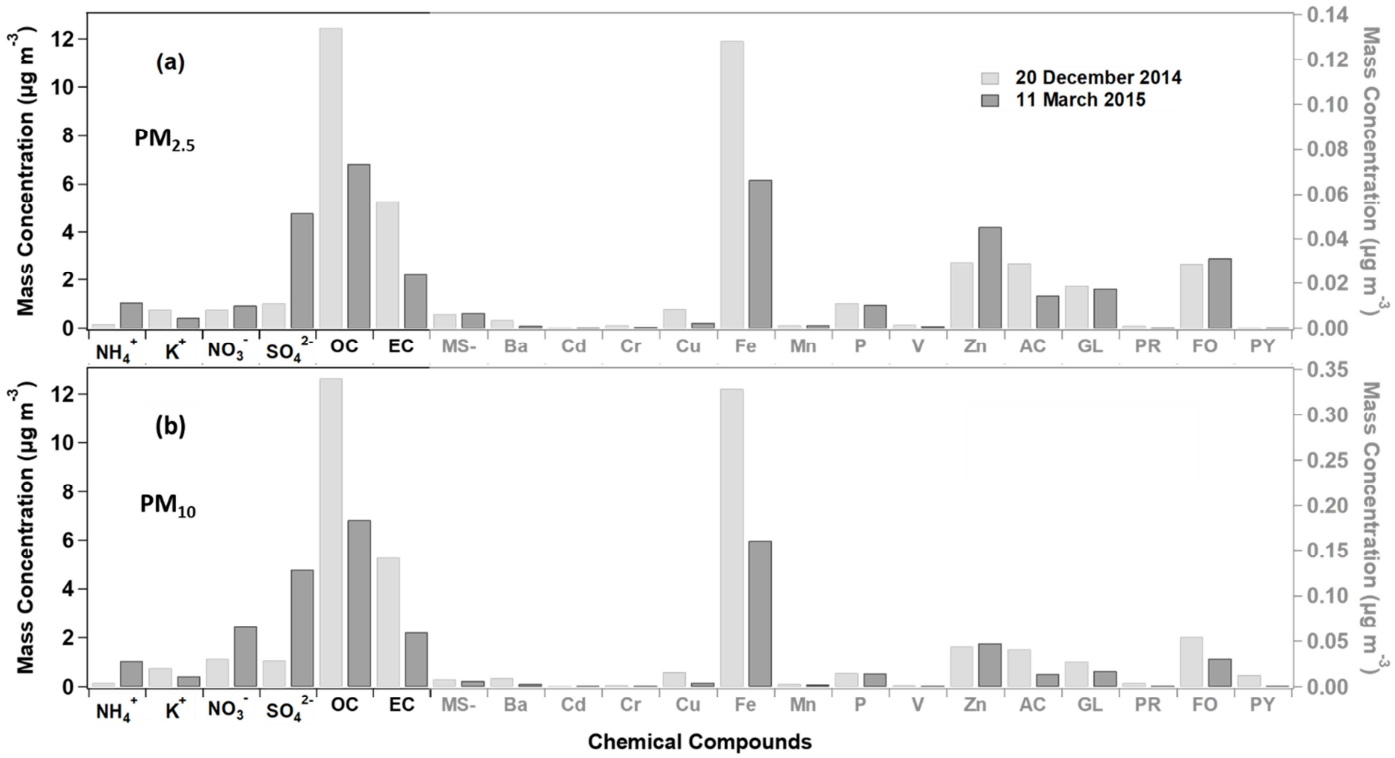

Figure 3. Mass concentration of the main redox active species monitored in the (a) $PM_{2.5}$ and (b) PM_{10} samples collected on 20 December 2014 and 11 March 2015 (light and dark grey bars, respectively). The chemical compounds marked in black and in grey are referred to the left and right y-axis, respectively. AC, GL, PR, FO, and PY represent the acetate, glycolate, propionate, formate, and pyruvate mass concentration.

807

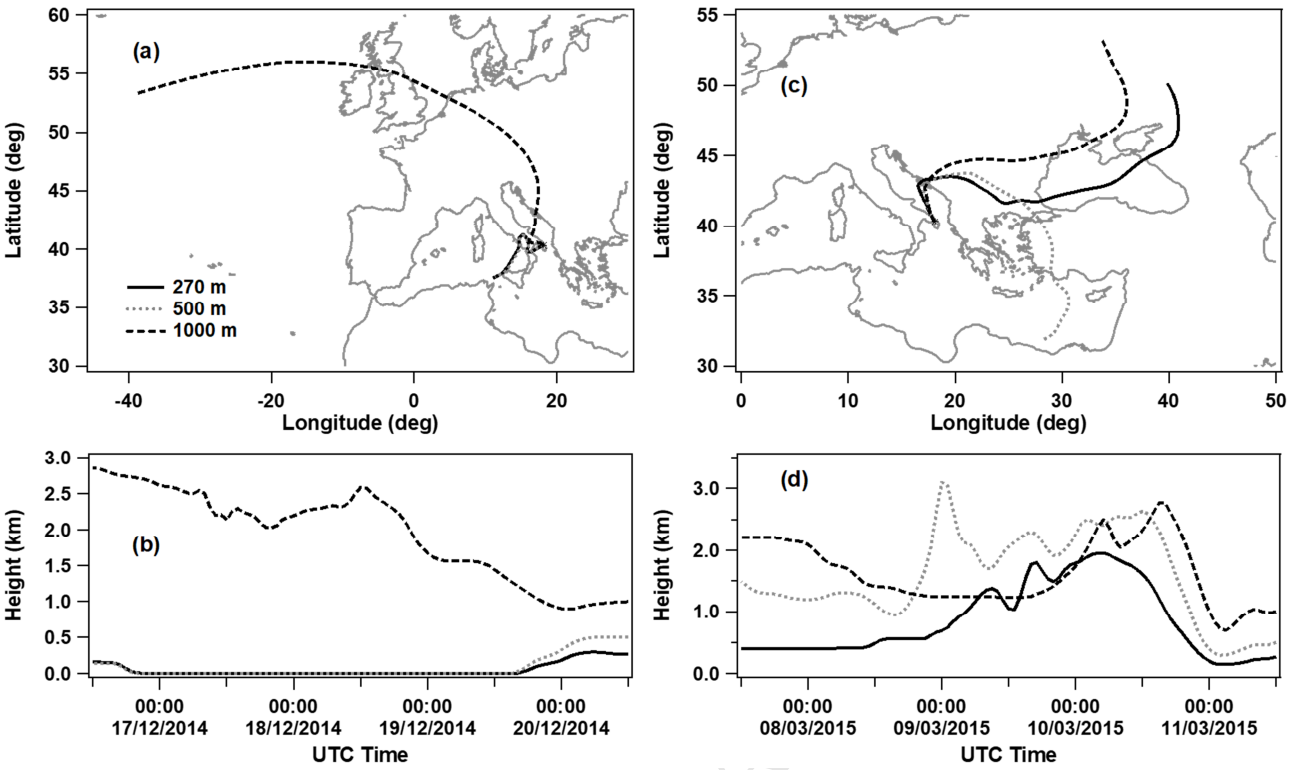

808

809

810

811

812 **Figure 4.** Four-day analytical back trajectories reaching the monitoring site (Lecce, Italy) at 270
813 (solid black line), 500 (dashed grey line), and 1000 m (dashed black line) above the ground level, at
814 12:00 UTC of (a) 20 December 2014 and (c) 11 March 2015. The altitude of each back trajectory as
815 a function of time is reported in (b) and (d) for the back trajectories plotted in (a) and (c),
816 respectively.

817

818

819

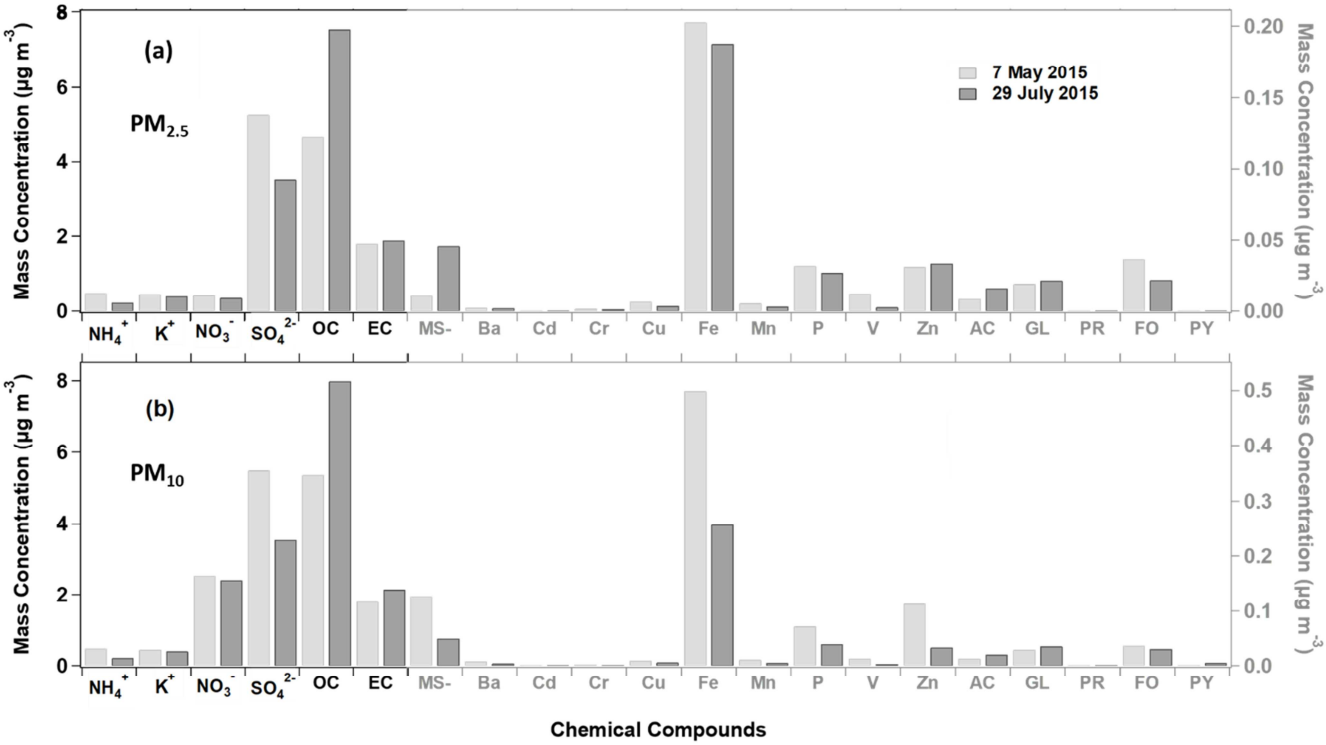

Figure 5. Mass concentration of the main redox active species monitored in the (a) $PM_{2.5}$ and (b) PM_{10} samples collected on 7 May and 29 July 2015 (light and dark grey bars, respectively). The chemical compounds marked in black and in grey are referred to the left and right y-axis, respectively. AC, GL, PR, FO, and PY represent the acetate, glycolate, propionate, formate, and pyruvate mass concentration.

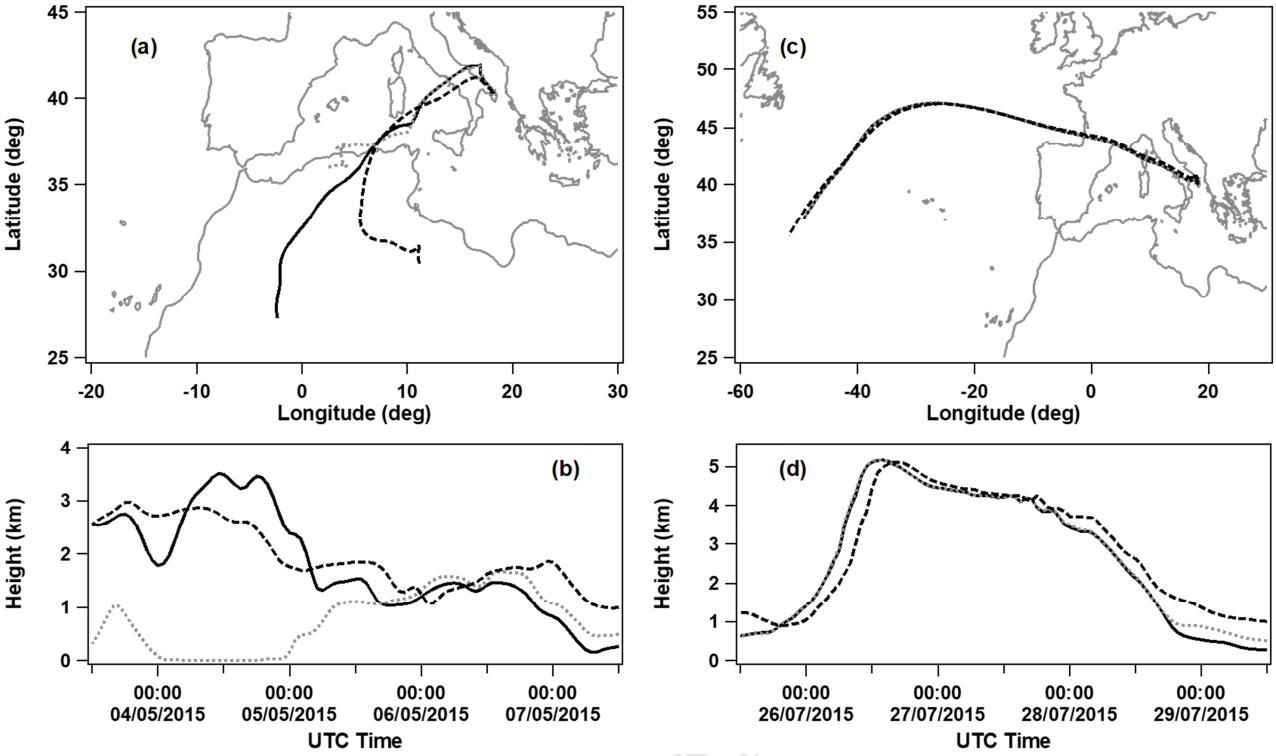

Figure 6. Four-day analytical back trajectories reaching the monitoring site (Lecce, Italy) at 270 (solid black line), 500 (dashed grey line), and 1000 m (dashed black line) above the ground level, at 12:00 UTC of (a) 7 May and (c) 29 July 2015. The altitude of each back trajectory as a function of time is reported in (b) and (d) for the back trajectories plotted in (a) and (c), respectively

Dear Dr. A Achuthan,

unfortunately we made some mistakes in the Figure Caption list at pg. 28 of the revised manuscript. In particular :

the Caption of Figure 2 :

"**Figure 2.** Daily evolution of the volume-normalized OP_V values in $PM_{2.5}$ and PM_{10} particles (dark and light grey bars, respectively). Figures 1a and 1b: OP^{AA}_V responses measured with DTT assay for Autumn-Winter (a) and Spring-Summer (b) periods; Figures 1c and 1d: OP^{DTT}_V responses measured with AA assay for Autumn-Winter (c) and Spring-Summer (d) periods; Figures 1e and 1f: temporal evolution of the $PM_{2.5}$ and PM_{10} mass concentration in Autumn-Winter (e) and Spring-Summer (f)."

should be replaced as follows:

" **Figure 2.** Temporal evolution of the volume-normalized oxidative potential (OP_V) values measured with the AA assay for (a) Autumn-Winter and (b) Spring-Summer, and the DTT assays for (c) Autumn-Winter and (d) Spring-Summer, for PM_{10} and $PM_{2.5}$ samples (light and dark grey bars, respectively). The temporal evolution of the PM_{10} and $PM_{2.5}$ concentration (light and dark grey bars, respectively) is also reported in (e) for Autumn-Winter and in (f) for Spring-Summer."

The Caption of Figure 3:

"**Figure 3.** Mass concentration of the main redox active species measured on 20 December 2014 and 11 March 2015 (light and dark grey bars, respectively) in $PM_{2.5}$ (a) and PM_{10} particles. The chemical compounds marked in black and in grey are referred to the left and right y-axis, respectively. AC, GL, PR, FO, and PY represent the acetate, glycolate, propionate, formate, and pyruvate mass concentration."

should be replaced as follows:

"**Figure 3.** Mass concentration of the main redox active species monitored in the (a) $PM_{2.5}$ and (b) PM_{10} samples collected on 20 December 2014 and 11 March 2015 (light and dark grey bars, respectively). The chemical compounds marked in black and in grey are referred to the left and right y-axis, respectively. AC, GL, PR, FO, and PY represent the acetate, glycolate, propionate, formate, and pyruvate mass concentration."

The Caption of Figure 4:

Figure 4. Four-day analytical back trajectories reaching the monitoring site (Lecce, Italy) at 270 (red), 500 (blue), and 1000 m (green) above the ground level, at 12:00 UTC of 20 December 2014 (a) and 11 March 2015 (c). Figures 3b and 3d: altitude of each back trajectory as a function of time on 20 December 2014 (a) and 11 March 2015 (c), respectively."

should be replaced as follows:

"**Figure 4.** Four-day analytical back trajectories reaching the monitoring site (Lecce, Italy) at 270 (solid black line), 500 (dashed grey line), and 1000 m (dashed black line) above the ground level, at 12:00 UTC of (a) 20 December 2014 and (c) 11 March 2015. The altitude of each back trajectory as a function of time is reported in (b) and (d) for the back trajectories plotted in (a) and (c), respectively."

The Caption of Figure 5:

"Figure 5. Mass concentration of the main redox active species measured on 7 May and 29 July 2015 (light and dark grey bars, respectively) in $PM_{2.5}$ (a) and PM_{10} particles. The chemical compounds marked in black and in grey are referred to the left and right y-axis, respectively. AC, GL, PR, FO, and PY represent the acetate, glycolate, propionate, formate, and pyruvate mass concentration."

should be replaced as follows:

Figure 5. Mass concentration of the main redox active species monitored in the (a) $PM_{2.5}$ and (b) PM_{10} samples collected on 7 May and 29 July 2015 (light and dark grey bars, respectively). The chemical compounds marked in black and in grey are referred to the left and right y-axis, respectively. AC, GL, PR, FO, and PY represent the acetate, glycolate, propionate, formate, and pyruvate mass concentration.

The Caption of Figure 6:

"Figure 6. Four-day analytical back trajectories reaching the monitoring site (Lecce, Italy) at 270 (red), 500 (blue), and 1000 m (green) above the ground level, at 12:00 UTC of 7 May (a) and 29 July 2015 (c). Figures 6b and 6d: altitude of each back trajectory as a function of time on 7 May (a) and 29 July 2015 (c), respectively."

should be replaced by:

"**Figure 6.** Four-day analytical back trajectories reaching the monitoring site (Lecce, Italy) at 270 (solid black line), 500 (dashed grey line), and 1000 m (dashed black line) above the ground level, at 12:00 UTC of (a) 7 May and (c) 29 July 2015. The altitude of each back trajectory as a function of time is reported in (b) and (d) for the back trajectories plotted in (a) and (c), respectively"

The captions reported at the botton of each figure are right.

Sorry for the problem,

Best regards,

Prof. M.C. Pietrogrande